Resident macrophages establish and control lipid stores via PDGFcc production

Nehemiah Cox[1*], Lucile Crozet[1,2*], Inge R. Holtman[3], Pierre-Louis Loyher[1], Tomi Lazarov[1], Elvira Mass[1,4], E. Richard Stanley[5], Christopher K. Glass[3], Frederic Geissmann[1,2&]
1. Immunology Program, Sloan Kettering Institute, Memorial Sloan Kettering Cancer Center, New York, New York 10065, USA.
2. Weill Cornell Graduate School of Medical Sciences, New York, New York 10065, USA.
3. Department of Cellular and Molecular Medicine, UCSD, San Diego, California, USA.
4. Developmental Biology of the Immune System, LIMES Institute, University of Bonn, 53115 Bonn, Germany.
5. Department of Developmental and Molecular Biology, Albert Einstein College of Medicine, Bronx, New York 10461, USA.

[*] These authors contributed equally
[&]Correspondence to geissmaf@mskcc.org

Summary

Metazoans have evolved specialized fat-storing tissues dedicated to the dynamic storage of energy. Fat tissues in mammals consist of lipid-storing adipocytes, macrophages, and stromal cells. Macrophages are tightly associated with adipocytes yet, their function in fat remains enigmatic. We report that resident, but not bone-marrow-derived, macrophages are critical for establishment and control of fat stores in metazoans. Mice lacking resident macrophages form adipocytes but fail to store lipids or to expand lipid stores in response to diet. Experiments in isolated fat-pads demonstrate that resident macrophages control fat storage via PDGFcc production in a tissue autonomous manner. Macrophage-derived PDGF-family growth factors in *Drosophila* larvae similarly act on fat cells to allow storage of lipid, demonstrating evolutionary conservation. We propose that resident macrophages, similar to adipocytes, are a critical component of the adipose tissue required for its function. Furthermore, our data suggest approaches to regulate adiposity by targeting resident macrophages and PDGFcc.

Main text

Daily and seasonal variation in caloric intake and activity results in cycles of energy storage and expenditure(Rosen and Spiegelman, 2006). Chordates have evolved dedicated tissues where specialized fat-storing cells accumulate surplus energy from diet, as triacylglycerols, and release fatty acids via lipolysis when expenditure exceeds intake(Hotamisligil, 2017; Rodeheffer et al., 2008; Rosen and Spiegelman, 2006; Wise, 1975) without the common lipotoxicity associated with fat accumulation in other tissues(Rodeheffer et al., 2008; Rosen and Spiegelman, 2006; Wise, 1975). Obesity and lipodystrophy are associated with a metabolic syndrome characterized by inflammation, insulin resistance, and type 2 diabetes(Arkan et al., 2005; Hotamisligil et al., 1995; Hotamisligil et al., 1993; Xu et al., 2003). This syndrome is attributable in part to lipid deposits outside the adipose tissue(Cai et al., 2005; Kraegen et al., 1991) and landmark studies from the 1980's onwards have established that the activation and recruitment of monocyte in obese adipose tissue and peripheral tissues such as the liver(Ito et al., 2008;

Parker et al., 2018) cause, and at times counteract(Jaitin et al., 2019), inflammation, lipid accumulation, insulin resistance, and type 2 diabetes in part via production of inflammatory cytokines such as TNF(Hirsch and Batchelor, 1976; Hotamisligil et al., 1995; Hotamisligil et al., 1993; Ito et al., 2008; Kamei et al., 2006; Kanda et al., 2006; Kim et al., 2016; McLaughlin et al., 2017; Obstfeld et al., 2010; Pekala et al., 1983; Suganami and Ogawa, 2010; Sullivan et al., 2013; Surmi and Hasty, 2008; Weisberg et al., 2006; Weisberg et al., 2003; Xu et al., 2003). Indeed, genetic or pharmacological inhibition of the *Ccr2*-dependent recruitment of monocytes to tissues prevents metabolic syndrome in obese mice(Kim et al., 2016; Obstfeld et al., 2010; Sullivan et al., 2013; Weisberg et al., 2006). HSC-derived *Ccr2*-dependent aacrophages are therefore considered a therapeutic target in metabolic diseases associated with obesity. However, macrophages are also present in lean adipose tissue where their roles remain poorly understood(Biswas and Mantovani, 2012; Debels et al., 2013; Han et al., 2011; Hotamisligil, 2017; Lee et al., 2013; McLaughlin et al., 2017; Pang et al., 2008; Pollard, 2009; Wei et al., 2005; Wernstedt Asterholm et al., 2014). It is proposed that macrophages are reprogrammed into an inflammatory phenotype in the setting of obese animals(Hotamisligil, 2017; Hume, 2015; Lumeng et al., 2007a; Lumeng et al., 2007b; McLaughlin et al., 2017; Nguyen et al., 2007; Odegaard et al., 2008; Pollard, 2009), although it is also suggested that they may protect mice against metabolic syndrome(Satoh et al., 2013; Wolf et al., 2017). Recognition of phenotypic and developmental heterogeneity(Coats et al., 2017; Gomez Perdiguero et al., 2015; Hassnain Waqas et al., 2017; Mass et al., 2016; Schulz et al., 2012; Silva et al., 2019; Zeyda et al., 2010) in adipose tissue macrophages lead to the hypothesis that distinct populations may mediate separate functions(Coats et al., 2017; Kratz et al., 2014; Silva et al., 2019; Zeyda et al., 2010). Here, we re-examined the roles of adipose macrophages in the context of their developmental origins, and identified an essential and evolutionarily conserved role of embryo-derived resident adipose tissue macrophages in establishment and control of lipid storage by specialized fat-storing tissues.

White adipose tissue deficiency in mice lacking Csf1r.

Mice carrying a homozygous deletion of the *Csf1* receptor (*Csf1r* $^{-/-}$ and *Csf1r*^{Cre}*; Csf1r*$^{f/f}$) lack macrophages in most tissues(Dai et al., 2002), including the fat-pads (**Figures 1A and S1),** and present with skeletal deformities (osteopetrosis) attributed to lack of osteoclasts(Dai et al., 2002; Jacome-Galarza et al., 2019) and abnormal brain development attributed to lack of microglia(Erblich et al., 2011). The weight of brain, lung, kidney and interscapular brown adipose tissue are no different between *Csf1r*-deficient and control littermates (**Figures S2A-C)**, however, both lines of *Csf1r*-deficient mice present with a 90% reduction in size and weight of visceral and sub-cutaneous white adipose tissues (WAT) at one month of life (**Figures 1B and S2A-C).** Of note, liver histology and size are normal in *Csf1r*-deficient mice (**Figure S2D**)**.** These results are in line with previous findings reported in *Csf1r* deficient rats(Pridans et al., 2018) and macrophage-deficient *Trib1* knockout mice(Satoh et al., 2013).

Lack of tissue resident macrophages account for white adipose tissue deficenicy in Csf1r-deficient mice.

Csf1r deletion in the *Flt3*-expressing hematopoietic stem cell lineage(Christensen and Weissman, 2001; Jacome-Galarza et al., 2019), and *Ccr2* deficiency, in which myeloid cell egress from the bone marrow and entry into WAT is minimal(Boring et al., 1997; Kim et al., 2016; Kurihara et al., 1997; Serbina and Pamer, 2006; Si et al., 2010; Tsou et al., 2007; Weisberg et al., 2006), both result in loss of small Tim4^{-} F4/80^{+} cells in white adipose tissue (**Figures 1A and S1C).** However, large Tim4^{+} F4/80^{+} cells are still present (**Figures**

1A and S1C), and white adipose tissue mass and histology are normal (**Figures 1C, S1C, and S2E-G**). Therefore, a deficiency in HSC-derived monocyte/macrophage is unlikely to account for the adipose tissue defect in *Csf1r*-deficient mice. In contrast, *Tnfrsf11a*^{Cre}*; Csf1r*$^{f/f}$ mice, as well as *Tnfrsf11a*^{Cre}*; PU.1*$^{f/f}$ mice, which both lack erythro-myeloid progenitors (EMP)-derived resident macrophages(Jacome-Galarza et al., 2019; Percin et al., 2018) and present with self-resolving osteopetrosis(Jacome-Galarza et al., 2019), lack large Tim4^{+} F4/80^{+} cells (**Figures 1A and S1C**) and recapitulate the adipose tissue phenotype of *Csf1r*$^{-/-}$ mice with a selective ~90% decrease in the weight of visceral and sub-cutaneous white adipose tissues in comparison to littermate controls (**Figures 1D,E and S3)**. Liver histology and liver triacylglycerols are unchanged in mutant *Tnfrsf11a*^{Cre}*; Csf1r*$^{f/f}$ mice as compared to littermate controls (**Figure 1F**)**.** Interscapular brown adipose tissue (iBAT) morphology and weight of mutant *Tnfrsf11a*^{Cre}*; Csf1r*$^{f/f}$ mice is also similar to controls, although thermogenesis-associated trasncripts such as *Ucp1, Dio2, Prdm16 and Cidea* are elevated in the iBAT (**Figures 1G, S3G, and S4A)**. In contrast, there is no increase in these thermogenesis-associated trasncripts in the iWAT of mutant mice (**Figures 1G and S4)**.

A lineage mapping analysis of E8.5 Csf1r^{+} EMPs, confirms post-natal labeling of large adipose tissue F4/80^{+} Tim4^{+} macrophages, but not of small F4/80^{+} Tim4^{-} cells (**Figure 1H**). *In situ* lineage-tracing analysis of *Csf1r*- and *Tnfrsf11a*- expressing cells in *Csf1r*^{Cre}; *Rosa26*$^{mT/mG}$ and *Tnfrsf11a*^{Cre}*; Rosa26*$^{mT/mG}$ mice show GFP expression by F4/80^{+} macrophages that surround adipocytes, while all other cells express membrane-bound tdTomato, indicating that Cre-recombinase activity only occurs in F4/80^{+} macrophages or their progenitors (**Figure S5)**. Moreover, GFP expression is restricted only to Tim4^{+} F4/80^{+} macrophages in *Tnfrsf11a*^{Cre}*; Rosa26*$^{mT/mG}$ mice, confirming the specific targeting of EMP-derived Tim4^{+} resident macrophages in the fat pads of *Tnfrsf11a*^{Cre}*; Csf1r*$^{f/f}$ mice (**Figure S5)**.

Altogether, these findings suggest that lack of EMP-derived resident macrophages is associated with reduced fat mass and increased iBAT acitivity (i.e. thermogenesis). Importantly, we find no signs of lipodystrophy or browning of the white adipose tissue in mutant *Tnfrsf11a*^{Cre}*; Csf1r*$^{f/f}$ mice. These data also indicate that HSC-derived *Ccr2*-dependent Tim4^{-} macrophages, which include Trem2+ macrophages(Jaitin et al., 2019) are neither required nor sufficient for white adipose tissue development in mice.

Adipocytes from mice lacking tissue resident macrophages fail to store lipids.

To distinguish between a storage defect or a lack of white adipocyte differentiation, we performed a time-course analysis of white adipose tissue development in mutant *Tnfrsf11a*^{Cre}*; Csf1r*$^{f/f}$ mice. Neonatal (P7) fat pads from *Tnfrsf11a*^{Cre}*; Csf1r*$^{f/f}$ mice and control littermates have similar weights (**Figures 2A and S3H)** and both contain small perilipin^{+} cells (**Figures 2B and S3B)**. However, mutant fat pads fail to grow during the first month of life as perilipin^{+} cells remain small in inguinal, epidydimal, and mesenteric fat pads (**Figures 2B-D and S3B,C).** A qPCR analysis indicate that adipocyte genes *Pparg*, *Adiponectin*, *Leptin, and Srebp1* are expressed at similar levels in P7 and P26 mutant fat-pads, albeit *Leptin* expression is decreased at P26 consistent with decreased lipid mass(Stern et al., 2016) (**Figure S4B)**. Whole-mount confocal analysis confirms that bodipy^{+} perilipin^{+} adipocytes are present in one month old *Tnfrsf11a*^{Cre}*;Csf1r*$^{f/f}$ fat pads, with a ~10-fold reduction in bodipy^{+} lipid content (**Figures 2C,D**), which corresponds to the 90% decrease in fat pad weight (**Figures 1E and 2A)**. Whole-mount confocal analysis also confirms that Tim4^{+} macrophages are absent from fat pads from *Tnfrsf11a*^{Cre}*;Csf1r*$^{f/f}$ mice in comparison to control littermates (**Figure 2C),** but CD31^{+} capillaries as well as PDGFRα^{+} stromal cells are still present (**Figures 2C,E)**. Therefore, the 90% reduction in

adipose tissue observed in *Tnfrsf11a^{Cre};Csf1r$^{f/f}$* mice may be accounted for by decreased storage of bodipy^{+} lipids in perilipin^{+} adipocytes, although these experiments do not eliminate the possible contribution of reduced proliferation/differentiation at the level of pre-adipocytes or perilipin-expressing cells.

Reduced PDGFcc in adipose tissue of mice lacking tissue resident macrophages.

Reduced lipid storage can reflect decreased nutrient intake or increased energy expenditure, as well as changes in growth factors that directly or indirectly control lipid storage in adipocyte (Boucher et al., 2016; Hu et al., 2015; Huang et al., 2009; Molgat et al., 2009; Onogi et al., 2017; Pang et al., 2008; Seki et al., 2018; Shook et al., 2018; Sottile and Seuwen, 2000). In support of the latter, a qPCR analysis of growth factors that control lipid storage in white adipocytes(Boucher et al., 2016; Hu et al., 2015; Huang et al., 2009; Molgat et al., 2009; Onogi et al., 2017; Pang et al., 2008; Seki et al., 2018; Shook et al., 2018; Sottile and Seuwen, 2000) indicate that expression of *Pdgfc and Igf1* are strongly reduced in fat pads from mutant mice as compared to control littermates (**Figure 2F)**. Expression of *Vegfb and Bmp2* is also reduced but to a lesser extent (**Figure 2F)**. A qPCR analysis of FACS-sorted adipose tissue macrophages indicate that wild-type Tim4^{+} resident macrophages express the pro-adipogenic growth factors *Pdgfc, Vegfb, Bmp2* and *Igf1* (**Figures 2G and S4C)**. Immunostaining with PDGFcc antibodies further demonstrate that ~90% of PDGFcc expressing cells are macrophages in *wt* iWAT, and that PDGFcc expression is not detectable in mutant fat pads that lack Tim4^{+} macrophages (**Figure 2H**), indicating that macrophages represent the main local source of PDGFcc in white adipose tissue. A possible role of PDGFcc is interesting as PDGF receptors alpha and beta have pleiotropic roles, including control of adipocyte differentiation and size(Gao et al., 2018; Sun et al., 2017; Vaziri and Faller, 1996). Altogether, the data above demonstrate that reduced white adipose tissue mass and adipocyte size in *Tnfrsf11a^{Cre}; Csf1r$^{f/f}$* mice is associated with a loss of pro-adipogenic growth factors produced by adipose tissue resident macrophages. We next performed a series of experiments to investigate whether reduced white adipocyte size is due to impaired lipid storage, decreased nutrient intake, and/or increased energy expenditure.

Macrophages control lipid storage in Drosophila fat body via PDGF signaling.

To directly test the roles of macrophage-derived growth factors in lipid storage, we first turned to *Drosophila* as a genetically tractable metazoan model. *Drosophila* does not exhibit any form of thermogenesis or fat tissue browning and decreased nutrient intake is always coupled to changes in timing of larval development. Hence, *Drosophila* represents an ideal model organism to invesitgate the function of macrophages in promoting lipid storage independently of their roles in food intake and thermogeneisis. Professional fat storing cells, macrophages, and the PDGF family of growth factors(Hoch and Soriano, 2003) are all conserved across the animal kingdom, including in *Drosophila*. Genetic labeling of *Drosophila* macrophages, hemocytes, with 2 independent reporters *Hml-gal4>uas-GFP(Clark et al., 2011)* and *Srp^{Hemo}-mCherry*(Bruckner et al., 2004; Gyoergy et al., 2018) confirm a close association between hemocytes and the dedicated fat storing tissue (fat body)(Zheng et al., 2017), labeled with *c564-gal4>uas-GFP*$^{+}$ (Franz et al., 2018; Kambris et al., 2006) in L3 larvae (**Figure 3A**). We thus generated hemocyte-deficient *Drosophila* by inducing apoptosis in hemocytes using *Srp^{Hemo}-gal4>uas-reaper* or *Hml-gal4 >uas-reaper* lines(Franz et al., 2018; Woodcock et al., 2015) *(Bruckner et al., 2004)* (**Figures 3B,C and S6A**). In both models, we observe a ~60% reduction in triglyceride content and fat body cell size as compared to control larvae (**Figures 3B,C**). This decrease is associated with reduced buoyancy(Reis et al., 2010) in hemocyte-deficient *Srp^{Hemo}-gal4>uas-reaper* wandering L3 larvae (**Figure 3D**).

We next investigated whether growth factors produced by *Drosophila* hemocytes(Brogiolo et al., 2001; Clark et al., 2011) **(Figure S6B**) are important for storage of triglycerides by fat body cells. Hemocyte-specific RNAi of *Bmp* (*Bmp*, *Daw), Igf* (*dilp5)*, and *Il1* (*Spätzle)* orthologs result in L3 larvae with normal triglyceride content and fat body cell size (**Figures 3E,F**). In contrast, hemocyte-specific RNAi of *Pvf3* (*Srp^{Hemo}-gal4>uas-pvf3-IR*) a PDGF family ortholog(Hoch and Soriano, 2003; Zheng et al., 2017) results in larvae with a ~60% decrease in triglyceride content and fat body cell size (**Figures 3E-G and S6C**). Larvae from hemocyte-specific *Pvf1* RNAi present with a milder phenotype: smaller fat body cells but no significant reduction in triglycerides (**Figures 3E,F and S6C**). PDGF/ family orthologs *Pvf3* and *Pvf1* share the receptor Pvr(Hoch and Soriano, 2003; Zheng et al., 2017), expressed by fat body cells(Leader et al., 2018)·(Zheng et al., 2017). As expected, RNAi of *Pvr* in the fat body, *c564-gal4>uas- pvr-IR,* yields L3 larvae with reduced triglyceride content and smaller fat body cells similar to hemocyte-deficient and *Pvf3 RNAi* larvae **(Figures 3H and S6D)**. To control for possible off-target effects of the RNAi constructs, we analyzed *Pvf3* mutant flies (*Pvf3^{EY09531}*). L3 *Pvf3^{EY09531}* larvae have reduced buoyancy and a ~70% reduction in triglyceride content and fat body cell size (**Figures 3I-K**). We also verified that genetic rescue of *Pvf3* expression in *Pvf3^{EY09531}* larvae restored triglyceride content and fat body cell size (*Pvf3^{EY09531}; He-gal4 (Zettervall et al., 2004)>uas-pvf3*) (**Figure 3K**). Finally, hemocyte-deficient L3 larvae present with a ~1 day developmental delay, but *Pvf3^{EY09531} and Srp^{Hemo}-gal4>uas-pvf3-IR* larvae develop in time and with normal size (**Figures S6E,F**). These data strongly suggest that *Drosophila* hemocytes control triglyceride storage in fat body cells via production of PDGF-family ortholog *Pvf3* by hemocytes acting directly on Pvr expressing fat body cells, and suggest an evolutionarily conserved role for growth factor produced by macrophages in control of lipid storage by fat storing cells.

PDGFcc produced by resident macrophages is required and sufficient for lipid storage by adipocytes in mouse fat-pad explants.

To determine in an orthogonal approach whether the role of resident macrophages and PDGF-family growth factors on lipid storage in mice can be observed independently of the systemic and pleotropic effects of macrophage depletion on nutrient intake and energy expenditure, we performed loss-of-function and rescue experiments in murine isolated fat-pad explants (**Figure 4A)**. Wild type murine neonatal (P4) epidydimal fat pad *anlagen* contain PDGFRα^+ cells, capillaries and macrophages, but lack perilipin$^+$, bodipy$^+$ or LipidTox$^+$ cells (**Figure 4B)**. As previously shown(Han et al., 2011), perilipin$^+$ bodipy$^+$ adipocytes develop *ex vivo* in 10 days from wild-type explant cultures with conventional non-adipogenic medium (**Figures 4C-E).** Perilipin$^+$ *Pparg$^+$* cells also develop in fat pad explants of *Tnfrsf11a^{Cre}; Csf1r$^{f/f}$* mice, but they contain little to no lipids as evidenced by scant bodipy staining as compared to fat-pads from control littermates (**Figures 4C-E).** Treatment of *Tnfrsf11a^{Cre}; Csf1r$^{f/f}$* fat pads with recombinant PDGFcc -but not IGF1- rescues bodipy staining and adipocyte size to control levels (**Figures 4F-H and S7A**). We observe that *in vitro* treatment with VEGFb can also rescue lipid storage (**Figure S7A**), suggesting that several macrophage growth factors may act directly and/or indirectly, e.g. via endothelial cells, to support lipid storage. Symmetrically, treatment of wild-type fat pads with anti-PDGFcc neutralizing antibodies (AF1447) phenocopy *Tnfrsf11a^{Cre}; Csf1r$^{f/f}$* fat-pad explants, with the development of small perilipin$^+$ *pparg$^+$* bodipy$^{low/neg}$ cells (**Figures 4G-I and S7B,C**). Altogther, our data demonstrate that macrophage deficiency or PDGFcc blockade in the presence of macrophages are both sufficient to prevent lipid storage by adipocytes in an isolated fat-pad explant, while PDGFcc supplementation is sufficient to rescue lipid storage by adipocytes even in the absence of macrophages.

These data thus indicate that, in an *ex-vivo* system, macrophages and PDGFcc support lipid storage by adipocytes in a white adipose tissue autonomous manner.

PDGFcc blockade prevents adipocyte hypertrophy.

The above data indicate that during development of fat stores PDGFcc and its PVF3 ortholog are important for lipid storage in dedicated fat storning cells e.g. murine white adipocytes and *Drosophila* fat body cells. To investigate the role of PDGFcc in adult mice, 6-week-old C57Bl/6J mice were treated with anti-PDGFcc neutralizing antibodies (AF1447, 10 µg/mouse, ip, thrice a week). This treatment does not deplete macrophages (**Figures S8A,B**). In mice fed a control diet (10% kCal from fat, 3.85 kCal/g), anti-PDGFcc antibodies does not decrease mouse weight (**Figure 5A**), fat tissue mass (**Figure 5B**), or adipocyte size (**Figure 5C,D**). However, in mice fed a lipid-rich diet (45% kCal from fat, 4.73 kCal/g) treatment with anti-PDGFcc antibodies abolishes weight gain (**Figure 5A**). Anti-PDGFcc treated mice remain lean under a lipid-rich diet as white adipose tissue mass (**Figure 5B**) and adipocyte size (**Figure 5C,D**) are comparable to lean controls. Anti-PDGFcc treatment does not modify food intake, fecal caloric density, and ambulatory daily activity (**Figures 5E,F and S8C**), however, energy expenditure is increased (**Figure 5G**). Anti-PDGFcc treatment does not induce browning of white adipose tissue (**Figures 5I and S8E,F**), but thermogenesis in interscapular brown adipose tissue is elevated as evidenced by increased surface body temperature (**Figure 5H**) and higher *Ucp1*, *Dio2, Prdm16 and Cidea*(de Jesus et al., 2001; Enerback et al., 1997) transcripts (**Figures 5I and S8D).** Importantly, anti-PDGFcc treatment alone does not increase thermogenesis in a mice fed a control diet (**Figures 5H,I**). Finally, this treatment does not modify ectopic lipid depostion in the liver (**Figures 5J,K**), liver inflammation (**Figure 5L**), or insulin resistance (**Figure S8G),** which are mediated by *Ccr2*-dependent inflammatory monocyte/macrophages(Ito et al., 2008; Kamei et al., 2006; Kanda et al., 2006; Kim et al., 2016; Obstfeld et al., 2010; Parker et al., 2018; Sullivan et al., 2013; Weisberg et al., 2006). These data altogether suggest that in PDGFcc is necessary for expansion of lipid stores in adult mice and that in the absence of PDGFcc under conditions of increased fat intake, excess lipids that are not stored in white adipose tissue are used for thermogenesis in the brown adipose tissue.

Lipid-rich diet up-regulates Pdgfc expression by resident macrophages in adult adipose tissue.

Fluorescence microscopy and flow cytometry analyses of F4/80$^+$ cells in visceral and subcutaneous white adipose tissue from adult mice (8 to 14 weeks) indicate that large F4/80$^+$ Tim4$^+$ macrophages are present in the adipose tissue of lean and obese adult mice (**Figures 6A,B and S9-11**). These F4/80$^+$ Tim4$^+$ macrophages are also present in similar numbers (~2x10^6.g^{-1} of tissue) in the adipose tissue of *Ccr2*-deficient mice or littermate controls (**Figures 6C and S11A**). F4/80$^+$ Tim4$^+$ macrophages do not exchange between mice in the course of 8-week long parabiosis (**Figures 6D and S11B)**, and they are labeled by Cre-mediated inducible lineage tracing of yolk sac EMPs(Gomez Perdiguero et al., 2015; Mass et al., 2016; Schulz et al., 2012) (**Figure S11C**) indicating that resident macrophages persist in adult adipose tissue**.** In contrast, small F4/80$^+$ Tim4$^-$ cells accumulate in fat pads of obese *wt* mice, forming crown-like structures (Suganami and Ogawa, 2010)(**Figures 6C and S11A,D**) but are missing from white adipose tissue of *Ccr2*-deficient mice (**Figures 6C and S11A,D**). These F4/80$^+$ Tim4$^-$ macrophages exchange between parabiotic mice (**Figures 6D and S11B**), and are not labeled by Cre-mediated inducible lineage tracing of yolk sac EMPs(Gomez Perdiguero et al., 2015; Mass et al., 2016; Schulz et al., 2012) **(Figure S11C**), suggesting that they correspond to HSC-derived monocyte/macrophages or monocyte-derived DCs. Transcriptional analysis indicate that EMP-derived Tim4$^+$ and HSC-derived Tim4$^-$ cells cells cluster by population

rather than diet in multidimensional scaling and hierarchical clustering of differentially expressed genes (**Figures 6e and S12, Table S1**). Tim4$^-$ monocyte/macrophages highly express genes associated with innate immune response and cell proliferation (Clusters 2 and 5 **Figure S12**) . A qPCR analysis confirms that they, and blood monocytes, are a source of TNF and IL-1b in mice that are fed excess lipids (45% fat) (**Figures 6F and S13**). Upon return to a standard diet (10% fat), the number of F4/80$^+$ Tim4$^-$ monocyte/macrophages returns to baseline within 2 weeks (**Figure S11E**). Concurrently, mouse body weight as well as their insulin resistance status return to a lean state (**Figures S11F-I**). Transcriptional analysis of resident F4/80$^+$ Tim4$^+$ macrophages indicate that, in contrast to small F4/80$^+$ Tim4$^-$ macrophages, these cells primarily express genes associated with homeostatic processes (Cluster 1, 7 **Figure S12**). A qPCR analysis of FACS-sorted cells confirms that F4/80$^+$ Tim4$^+$ macrophages are the main source of adipogenic growth factors, including *Pdgfc,* the expression of which is upregulated on lipid rich diet (**Figures 6F and S13A,B**). The analysis of genes associated with M1 or M2 polarization of macrophages(Shaul et al., 2010) do not indicate an apparent polarization of macrophage in response to dietary changes (**Figures S13C,D**).

These data altogether indicate that resident F4/80$^+$ Tim4$^+$ and HSC-derived F4/80$^+$ Tim4$^-$ cells co-exist in the same adipose tissue, but are nonetheless characterized by distinct phenotypes and cellular dynamics. Furthermore, gene expression analysis is consistent with the known inflammatory role for Tim4$^-$ monocyte/macrophages and a novel homeostatic/pro-adipogenic role for F4/80$^+$ Tim4$^+$ adipose resident macrophages.

Deletion of macrophages in adult wt and db/db mice prevents Pdgfc up-regulation and adipocytes hypertrophy.

To further investigate the role of resident macrophages in adult mice, we compared the effect of *Ccr2*-deficiency(Boring et al., 1997) and CSF1R blockade on adipose tissue expansion in obese animals. *Ccr2*-deficient mice lack HSC-derived adipose tissue macrophages and when fed a lipid rich diet are protected against hepatic steatosis, monocyte recruitment, inflammation, and the metabolic syndrome(Ito et al., 2008; Kamei et al., 2006; Kanda et al., 2006; Sullivan et al., 2013; Weisberg et al., 2006). In accordance with these previous observations, *Ccr2*-deficient mice fed a lipid rich diet are protected against accumulation of F4/80$^+$ Tim4$^-$ monocyte/macrophages (**Figure 6C)**, CLS formation, and the metabolic syndrome **(Figure S14A,B**). However, we found that *Ccr2*-deficient mice gain weight to the same extent as control mice **(Figure S14C**), and Tim4$^+$ adipose tissue macrophages (**Figure 6C),** *Pdgfc* expression in fat tissue (**Figure 6G)**, fat mass (**Figure 6F)**, and adipocyte hypertrophy (**Figures 6I,J and S14D)** are no different in *Ccr2*-deficient mice and control littermates.

Mice treated with the CSF1R inhibitor, PLX5622 (1,200 mg PLX5622/kg of food), lack both HSC-derived Tim4$^-$ and EMP-derived Tim4$^+$ macrophages (**Figures S14E,F**). These mice, similar to *Ccr2*-deficient mice, are protected against TNF/IL1 production, hepatic steatosis, and the metabolic syndrome ((Valdearcos et al., 2014) **Figures S14G-K).** However, unlike *Ccr2*-deficient mice, they gain less weight when fed a lipid rich diet (**Figure S14L).** PLX5622 treatment reduces *Pdgfc* expression (**Figure 6G),** visceral and subcutaneous white adipose tissue mass (**Figure 6H),** and adipocyte size in mice fed a lipid rich diet (**Figures 6I,K**). Food intake, fecal caloric density, or ambulatory acitvity are no different in PLX5622-treated and control mice (**Figures 6L,M and S14M,N**). Importantly, similar to anti-PDGFcc treated mice, there are no signs of adipose tissue browning, but iBAT activty is increased (**Figures 6N and S15).** To control for off-target effects of the tyrosine kinase inhibitor, PLX5622, mice were also treated with a blocking anti-CSF1R antibody (AFS98(Sudo et al., 1995), 50 mg/kg, ip, thrice a week). AFS98 treatement deplets

adipose tissue macrophage -but not microglia- (**Figures S14E,F).** Anti-CSF1R antibody injections, similar to PLX5622 treatment, reduces *Pdgfc* expression (**Figure 6G),** adipose tissue mass (**Figure 6H)**, and adipocyte size in mice fed a lipid rich diet as compared to controls (**Figure 6I,K)**. Therefore, in addition to the effects of *Ccr2* deficiency, CSF1R inihibtition also recapitulates the effects of PDGFcc blockade, confirming that resident macrophages are required for increased *Pdgfc* production and storage of excess lipid in adipocytes in coditions of excess lipid intake.

To investigate the involvement of leptin signaling(Valdearcos et al., 2017; Valdearcos et al., 2014) and the roles of resident macrophages in storage of excess lipids in hyperphagic mice fed a control diet, we analysed leptin-receptor deficient mice (*Lepr$^{-/-}$, db/db*) that spontaneously develop obesity. We found that PLX5622 treatment limits weight gain (**Figure S16A**), reduces *Pdgfc* expression in the adipose tissue (**Figure 6O**), decreases adipose tissue mass (**Figure S16B)** and adipocyte size (**Figure 6P),** as well as liver inflammation **(Figures S16C-F).** PLX5622 treatment in *Lepr$^{-/-}$* mice also increases *Ucp1* and *Dio2* expression in the iBAT (**Figure S16G)**, but does not detectably modify ambulatory activity **(Figure S16H),** food intake (**Figure S16I),** or fecal caloric density (**Figure S16J**) in comparison to untreated controls, indicating that resident macrophages and PDGFcc may also control storage of excess lipids in hyperphagic mice, at least in part, independently of leptin signalling.

Discussion

We report here observations which indicate that PDGF family growth factors produced by resident macrophages in response to dietary changes mediate the storage of excess lipids in specialized fat cells from early post-natal mice and *Drosophila* larva, as well as hyperphagic and lipid-rich-diet fed adult mice. Consistent data across 4 different models: neonatal mice, *Drosophila* larvae devoid of thermogenesis, isolated fat pad explants submitted to loss-of-function and rescue experiments, and *wt* and *db/db* adult mice treated with anti-PDGFcc neutralizing antibodies or CSF1R1 inibitors, all indicate that PDGFcc controls lipid storage in adipocytes, and that the lean phenotypes observed in the absence of macrophages or PDGFcc is not secondary to decreased nutrient intake, malabsorption, white adipose tissue browning, or increased thermogenesis. It is important to note that anti-PDGFcc treatment does not increase thermogenesis or induce brownisation in a wild-type mice fed a control diet.

As this surprizing function of resident macrophages, *i.e.* promoting lipid storage in specialized fat cells in condition of excess nutrient intake, appears to be evolutionarily conserved in mice and *Drosophila*, we propose that macrophages and specialized fat-storing cells constitute a functional unit in metazoans, where macrophages sense the organism's nutritional state (Remmerie and Scott, 2018) and signal increased lipid storage to adipocytes through regulated paracrine production of PDGF family growth factors. *Drosophila* do not have fibroblasts or endothelial cells in the fat body, and *Pvr* silencing in fat cells phenocopies *Pvf3* silencing in hemocytes, suggesting that the interaction between macrophages and fat cells may be a direct one in flies. Nevertheless, further mechanistic studies in mice directed at investigating the roles of macrophage-derived PDGFcc and other growth factors on endothelium and stromal cells for the purpose of fat storage are warranted since for example a role of endothelial cells cannot be eliminated in mice. More importantly, PDGF-receptor signaling plays complex and at time opposing roles in lipid storage(Gao et al., 2018; Haider et al., 2018; Onogi et al., 2017; Sun et al., 2017; Vaziri and Faller, 1996), and the downstream molecular mechanisms involved in the control of lipid storage and energy expenditure by PDGF signaling in fat cells are not characterized.

Macrophage developmental and phenotypic heterogeneity in mice has long been suspected to underlie specialized functions attributable to different macrophage cell types. In contrast to resident macrophages, HSC-derived Tim4^{-} monocyte/macrophages, which include Trem2+ macrophages(Jaitin et al., 2019), are neither required, nor sufficient, for fat storage in white adipose tissue, while they are required in obese animals to mediate TNF and IL-1 production, hepatic steatosis, and metabolic syndrome(Ito et al., 2008; Kamei et al., 2006; Kanda et al., 2006; Kim et al., 2016; Obstfeld et al., 2010; Parker et al., 2018; Sullivan et al., 2013; Weisberg et al., 2006). Accordingly we find that resident macrophages are not sufficient to mediate systemic inflammation, ectopic deposition of lipids, and metabolic syndrome. Therefore, our data do not support a model where inflammation and insulin resistance in mice would be controlled by the reprogramming of resident macrophages from a homeostatic into a pro-inflammatory role in the setting of metabolic stress. Instead, distinct developmental subsets, *i.e.* resident macrophages and recruited HSC derived monocyte/macrophages perform distinct functions in the adipose tissue 'niche' and may be targeted independently by CCR2 and/or PDGFcc blockade.

Altogether, the present study identifies a mechanism that controls the expansion of fat stores in metazoans, in the context of a cellular 'dissection' of macrophage functions in lipid metabolism. Our data suggest pharmacological approaches that may help in regulating fat stores and preventing metabolic diseases in pathological conditions such as morbid obesity or cachexia.

References

Arkan, M.C., Hevener, A.L., Greten, F.R., Maeda, S., Li, Z.W., Long, J.M., Wynshaw-Boris, A., Poli, G., Olefsky, J., and Karin, M. (2005). IKK-beta links inflammation to obesity-induced insulin resistance. Nature medicine *11*, 191-198.

Biswas, S.K., and Mantovani, A. (2012). Orchestration of metabolism by macrophages. Cell metabolism *15*, 432-437.

Boring, L., Gosling, J., Chensue, S.W., Kunkel, S.L., Farese, R.V., Jr., Broxmeyer, H.E., and Charo, I.F. (1997). Impaired monocyte migration and reduced type 1 (Th1) cytokine responses in C-C chemokine receptor 2 knockout mice. The Journal of clinical investigation *100*, 2552-2561.

Boucher, J., Softic, S., El Ouaamari, A., Krumpoch, M.T., Kleinridders, A., Kulkarni, R.N., O'Neill, B.T., and Kahn, C.R. (2016). Differential Roles of Insulin and IGF-1 Receptors in Adipose Tissue Development and Function. Diabetes *65*, 2201-2213.

Brogiolo, W., Stocker, H., Ikeya, T., Rintelen, F., Fernandez, R., and Hafen, E. (2001). An evolutionarily conserved function of the Drosophila insulin receptor and insulin-like peptides in growth control. Curr Biol *11*, 213-221.

Bruckner, K., Kockel, L., Duchek, P., Luque, C.M., Rorth, P., and Perrimon, N. (2004). The PDGF/VEGF receptor controls blood cell survival in Drosophila. Developmental cell *7*, 73-84.

Cai, D., Yuan, M., Frantz, D.F., Melendez, P.A., Hansen, L., Lee, J., and Shoelson, S.E. (2005). Local and systemic insulin resistance resulting from hepatic activation of IKK-beta and NF-kappaB. Nature medicine *11*, 183-190.

Christensen, J.L., and Weissman, I.L. (2001). Flk-2 is a marker in hematopoietic stem cell differentiation: a simple method to isolate long-term stem cells. Proceedings of the National Academy of Sciences of the United States of America *98*, 14541-14546.

Clark, R.I., Woodcock, K.J., Geissmann, F., Trouillet, C., and Dionne, M.S. (2011). Multiple TGF-beta superfamily signals modulate the adult Drosophila immune response. Curr Biol *21*, 1672-1677.

Coats, B.R., Schoenfelt, K.Q., Barbosa-Lorenzi, V.C., Peris, E., Cui, C., Hoffman, A., Zhou, G., Fernandez, S., Zhai, L., Hall, B.A.*, et al.* (2017). Metabolically Activated Adipose Tissue Macrophages Perform Detrimental and Beneficial Functions during Diet-Induced Obesity. Cell reports *20*, 3149-3161.

Dai, X.M., Ryan, G.R., Hapel, A.J., Dominguez, M.G., Russell, R.G., Kapp, S., Sylvestre, V., and Stanley, E.R. (2002). Targeted disruption of the mouse colony-stimulating factor 1 receptor gene results in osteopetrosis, mononuclear phagocyte deficiency, increased primitive progenitor cell frequencies, and reproductive defects. Blood *99*, 111-120.

de Jesus, L.A., Carvalho, S.D., Ribeiro, M.O., Schneider, M., Kim, S.W., Harney, J.W., Larsen, P.R., and Bianco, A.C. (2001). The type 2 iodothyronine deiodinase is

essential for adaptive thermogenesis in brown adipose tissue. The Journal of clinical investigation *108*, 1379-1385.

Debels, H., Galea, L., Han, X.L., Palmer, J., van Rooijen, N., Morrison, W., and Abberton, K. (2013). Macrophages play a key role in angiogenesis and adipogenesis in a mouse tissue engineering model. Tissue Eng Part A *19*, 2615-2625.

Enerback, S., Jacobsson, A., Simpson, E.M., Guerra, C., Yamashita, H., Harper, M.E., and Kozak, L.P. (1997). Mice lacking mitochondrial uncoupling protein are cold-sensitive but not obese. Nature *387*, 90-94.

Erblich, B., Zhu, L., Etgen, A.M., Dobrenis, K., and Pollard, J.W. (2011). Absence of colony stimulation factor-1 receptor results in loss of microglia, disrupted brain development and olfactory deficits. PloS one *6*, e26317.

Franz, A., Wood, W., and Martin, P. (2018). Fat Body Cells Are Motile and Actively Migrate to Wounds to Drive Repair and Prevent Infection. Developmental cell *44*, 460-470 e463.

Gao, Z., Daquinag, A.C., Su, F., Snyder, B., and Kolonin, M.G. (2018). PDGFRalpha/PDGFRbeta signaling balance modulates progenitor cell differentiation into white and beige adipocytes. Development *145*.

Gomez Perdiguero, E., Klapproth, K., Schulz, C., Busch, K., Azzoni, E., Crozet, L., Garner, H., Trouillet, C., de Bruijn, M.F., Geissmann, F.*, et al.* (2015). Tissue-resident macrophages originate from yolk-sac-derived erythro-myeloid progenitors. Nature *518*, 547-551.

Gyoergy, A., Roblek, M., Ratheesh, A., Valoskova, K., Belyaeva, V., Wachner, S., Matsubayashi, Y., Sanchez-Sanchez, B.J., Stramer, B., and Siekhaus, D.E. (2018). Tools Allowing Independent Visualization and Genetic Manipulation of Drosophila melanogaster Macrophages and Surrounding Tissues. G3 (Bethesda) *8*, 845-857.

Haider, N., Dusseault, J., and Larose, L. (2018). Nck1 Deficiency Impairs Adipogenesis by Activation of PDGFRalpha in Preadipocytes. iScience *6*, 22-37.

Han, J., Lee, J.E., Jin, J., Lim, J.S., Oh, N., Kim, K., Chang, S.I., Shibuya, M., Kim, H., and Koh, G.Y. (2011). The spatiotemporal development of adipose tissue. Development *138*, 5027-5037.

Hassnain Waqas, S.F., Noble, A., Hoang, A.C., Ampem, G., Popp, M., Strauss, S., Guille, M., and Roszer, T. (2017). Adipose tissue macrophages develop from bone marrow-independent progenitors in Xenopus laevis and mouse. Journal of leukocyte biology *102*, 845-855.

Hirsch, J., and Batchelor, B. (1976). Adipose tissue cellularity in human obesity. Clin Endocrinol Metab *5*, 299-311.

Hoch, R.V., and Soriano, P. (2003). Roles of PDGF in animal development. Development *130*, 4769-4784.

Hotamisligil, G.S. (2017). Foundations of Immunometabolism and Implications for Metabolic Health and Disease. Immunity *47*, 406-420.

Hotamisligil, G.S., Arner, P., Caro, J.F., Atkinson, R.L., and Spiegelman, B.M. (1995). Increased adipose tissue expression of tumor necrosis factor-alpha in human obesity and insulin resistance. J Clin Invest *95*, 2409-2415.

Hotamisligil, G.S., Shargill, N.S., and Spiegelman, B.M. (1993). Adipose expression of tumor necrosis factor-alpha: direct role in obesity-linked insulin resistance. Science *259*, 87-91.

Hu, L., Yang, G., Hagg, D., Sun, G., Ahn, J.M., Jiang, N., Ricupero, C.L., Wu, J., Rodhe, C.H., Ascherman, J.A.*, et al.* (2015). IGF1 Promotes Adipogenesis by a Lineage Bias of Endogenous Adipose Stem/Progenitor Cells. Stem Cells *33*, 2483-2495.

Huang, H., Song, T.J., Li, X., Hu, L., He, Q., Liu, M., Lane, M.D., and Tang, Q.Q. (2009). BMP signaling pathway is required for commitment of C3H10T1/2 pluripotent stem cells to the adipocyte lineage. Proc Natl Acad Sci U S A *106*, 12670-12675.

Hume, D.A. (2015). The Many Alternative Faces of Macrophage Activation. Frontiers in immunology *6*, 370.

Ito, A., Suganami, T., Yamauchi, A., Degawa-Yamauchi, M., Tanaka, M., Kouyama, R., Kobayashi, Y., Nitta, N., Yasuda, K., Hirata, Y.*, et al.* (2008). Role of CC chemokine receptor 2 in bone marrow cells in the recruitment of macrophages into obese adipose tissue. J Biol Chem *283*, 35715-35723.

Jacome-Galarza, C.E., Percin, G.I., Muller, J.T., Mass, E., Lazarov, T., Eitler, J., Rauner, M., Yadav, V.K., Crozet, L., Bohm, M.*, et al.* (2019). Developmental origin, functional maintenance and genetic rescue of osteoclasts. Nature.

Jaitin, D.A., Adlung, L., Thaiss, C.A., Weiner, A., Li, B., Descamps, H., Lundgren, P., Bleriot, C., Liu, Z., Deczkowska, A.*, et al.* (2019). Lipid-Associated Macrophages Control Metabolic Homeostasis in a Trem2-Dependent Manner. Cell *178*, 686-698 e614.

Kambris, Z., Brun, S., Jang, I.H., Nam, H.J., Romeo, Y., Takahashi, K., Lee, W.J., Ueda, R., and Lemaitre, B. (2006). Drosophila immunity: a large-scale in vivo RNAi screen identifies five serine proteases required for Toll activation. Current biology : CB *16*, 808-813.

Kamei, N., Tobe, K., Suzuki, R., Ohsugi, M., Watanabe, T., Kubota, N., Ohtsuka-Kowatari, N., Kumagai, K., Sakamoto, K., Kobayashi, M.*, et al.* (2006). Overexpression of monocyte chemoattractant protein-1 in adipose tissues causes macrophage recruitment and insulin resistance. J Biol Chem *281*, 26602-26614.

Kanda, H., Tateya, S., Tamori, Y., Kotani, K., Hiasa, K., Kitazawa, R., Kitazawa, S., Miyachi, H., Maeda, S., Egashira, K.*, et al.* (2006). MCP-1 contributes to macrophage infiltration into adipose tissue, insulin resistance, and hepatic steatosis in obesity. J Clin Invest *116*, 1494-1505.

Kim, J., Chung, K., Choi, C., Beloor, J., Ullah, I., Kim, N., Lee, K.Y., Lee, S.K., and Kumar, P. (2016). Silencing CCR2 in Macrophages Alleviates Adipose Tissue Inflammation and the Associated Metabolic Syndrome in Dietary Obese Mice. Mol Ther Nucleic Acids *5*, e280.

Kraegen, E.W., Clark, P.W., Jenkins, A.B., Daley, E.A., Chisholm, D.J., and Storlien, L.H. (1991). Development of muscle insulin resistance after liver insulin resistance in high-fat-fed rats. Diabetes *40*, 1397-1403.

Kratz, M., Coats, B.R., Hisert, K.B., Hagman, D., Mutskov, V., Peris, E., Schoenfelt, K.Q., Kuzma, J.N., Larson, I., Billing, P.S.*, et al.* (2014). Metabolic dysfunction drives a mechanistically distinct proinflammatory phenotype in adipose tissue macrophages. Cell metabolism *20*, 614-625.

Kurihara, T., Warr, G., Loy, J., and Bravo, R. (1997). Defects in Macrophage Recruitment and Host Defense in Mice Lacking the CCR2 Chemokine Receptor. The Journal of experimental medicine *186*, 1757-1762.

Leader, D.P., Krause, S.A., Pandit, A., Davies, S.A., and Dow, J.A.T. (2018). FlyAtlas 2: a new version of the Drosophila melanogaster expression atlas with RNA-Seq, miRNA-Seq and sex-specific data. Nucleic Acids Res *46*, D809-D815.

Lee, Y.H., Petkova, A.P., and Granneman, J.G. (2013). Identification of an adipogenic niche for adipose tissue remodeling and restoration. Cell Metab *18*, 355-367.

Lumeng, C.N., Bodzin, J.L., and Saltiel, A.R. (2007a). Obesity induces a phenotypic switch in adipose tissue macrophage polarization. The Journal of clinical investigation *117*, 175-184.

Lumeng, C.N., Deyoung, S.M., Bodzin, J.L., and Saltiel, A.R. (2007b). Increased inflammatory properties of adipose tissue macrophages recruited during diet-induced obesity. Diabetes *56*, 16-23.

Mass, E., Ballesteros, I., Farlik, M., Halbritter, F., Gunther, P., Crozet, L., Jacome-Galarza, C.E., Handler, K., Klughammer, J., Kobayashi, Y.*, et al.* (2016). Specification of tissue-resident macrophages during organogenesis. Science *353*.

McLaughlin, T., Ackerman, S.E., Shen, L., and Engleman, E. (2017). Role of innate and adaptive immunity in obesity-associated metabolic disease. The Journal of clinical investigation *127*, 5-13.

Molgat, A.S., Gagnon, A., and Sorisky, A. (2009). Preadipocyte apoptosis is prevented by macrophage-conditioned medium in a PDGF-dependent manner. American journal of physiology Cell physiology *296*, C757-765.

Nguyen, M.T., Favelyukis, S., Nguyen, A.K., Reichart, D., Scott, P.A., Jenn, A., Liu-Bryan, R., Glass, C.K., Neels, J.G., and Olefsky, J.M. (2007). A subpopulation of macrophages infiltrates hypertrophic adipose tissue and is activated by free fatty acids via Toll-like receptors 2 and 4 and JNK-dependent pathways. The Journal of biological chemistry *282*, 35279-35292.

Obstfeld, A.E., Sugaru, E., Thearle, M., Francisco, A.M., Gayet, C., Ginsberg, H.N., Ables, E.V., and Ferrante, A.W., Jr. (2010). C-C chemokine receptor 2 (CCR2) regulates the hepatic recruitment of myeloid cells that promote obesity-induced hepatic steatosis. Diabetes *59*, 916-925.

Odegaard, J.I., Ricardo-Gonzalez, R.R., Red Eagle, A., Vats, D., Morel, C.R., Goforth, M.H., Subramanian, V., Mukundan, L., Ferrante, A.W., and Chawla, A. (2008). Alternative M2 Activation of Kupffer Cells by PPARδ Ameliorates Obesity-Induced Insulin Resistance. Cell metabolism *7*, 496-507.

Onogi, Y., Wada, T., Kamiya, C., Inata, K., Matsuzawa, T., Inaba, Y., Kimura, K., Inoue, H., Yamamoto, S., Ishii, Y.*, et al.* (2017). PDGFRbeta Regulates Adipose Tissue Expansion and Glucose Metabolism via Vascular Remodeling in Diet-Induced Obesity. Diabetes *66*, 1008-1021.

Pang, C., Gao, Z., Yin, J., Zhang, J., Jia, W., and Ye, J. (2008). Macrophage infiltration into adipose tissue may promote angiogenesis for adipose tissue remodeling in obesity. American journal of physiology Endocrinology and metabolism *295*, E313-322.

Parker, R., Weston, C.J., Miao, Z., Corbett, C., Armstrong, M.J., Ertl, L., Ebsworth, K., Walters, M.J., Baumart, T., Newland, D.*, et al.* (2018). CC chemokine receptor 2 promotes recruitment of myeloid cells associated with insulin resistance in nonalcoholic fatty liver disease. Am J Physiol Gastrointest Liver Physiol *314*, G483-G493.

Pekala, P., Kawakami, M., Vine, W., Lane, M.D., and Cerami, A. (1983). Studies of insulin resistance in adipocytes induced by macrophage mediator. J Exp Med *157*, 1360-1365.

Percin, G.I., Eitler, J., Kranz, A., Fu, J., Pollard, J.W., Naumann, R., and Waskow, C. (2018). CSF1R regulates the dendritic cell pool size in adult mice via embryo-derived tissue-resident macrophages. Nature Communications *9*.

Pollard, J.W. (2009). Trophic macrophages in development and disease. Nature reviews Immunology *9*, 259-270.

Pridans, C., Raper, A., Davis, G.M., Alves, J., Sauter, K.A., Lefevre, L., Regan, T., Meek, S., Sutherland, L., Thomson, A.J.*, et al.* (2018). Pleiotropic Impacts of Macrophage and Microglial Deficiency on Development in Rats with Targeted Mutation of the Csf1r Locus. J Immunol *201*, 2683-2699.

Reis, T., Van Gilst, M.R., and Hariharan, I.K. (2010). A buoyancy-based screen of Drosophila larvae for fat-storage mutants reveals a role for Sir2 in coupling fat storage to nutrient availability. PLoS Genet *6*, e1001206.

Remmerie, A., and Scott, C.L. (2018). Macrophages and lipid metabolism. Cellular immunology *330*, 27-42.

Rodeheffer, M.S., Birsoy, K., and Friedman, J.M. (2008). Identification of white adipocyte progenitor cells in vivo. Cell *135*, 240-249.

Rosen, E.D., and Spiegelman, B.M. (2006). Adipocytes as regulators of energy balance and glucose homeostasis. Nature *444*, 847-853.

Satoh, T., Kidoya, H., Naito, H., Yamamoto, M., Takemura, N., Nakagawa, K., Yoshioka, Y., Morii, E., Takakura, N., Takeuchi, O.*, et al.* (2013). Critical role of Trib1 in differentiation of tissue-resident M2-like macrophages. Nature *495*, 524-528.

Schulz, C., Gomez Perdiguero, E., Chorro, L., Szabo-Rogers, H., Cagnard, N., Kierdorf, K., Prinz, M., Wu, B., Jacobsen, S.E., Pollard, J.W.*, et al.* (2012). A lineage of myeloid cells independent of Myb and hematopoietic stem cells. Science *336*, 86-90.

Seki, T., Hosaka, K., Fischer, C., Lim, S., Andersson, P., Abe, M., Iwamoto, H., Gao, Y., Wang, X., Fong, G.H.*, et al.* (2018). Ablation of endothelial VEGFR1 improves metabolic dysfunction by inducing adipose tissue browning. J Exp Med *215*, 611-626.

Serbina, N.V., and Pamer, E.G. (2006). Monocyte emigration from bone marrow during bacterial infection requires signals mediated by chemokine receptor CCR2. Nature immunology *7*, 311-317.

Shaul, M.E., Bennett, G., Strissel, K.J., Greenberg, A.S., and Obin, M.S. (2010). Dynamic, M2-like remodeling phenotypes of CD11c+ adipose tissue macrophages during high-fat diet--induced obesity in mice. Diabetes *59*, 1171-1181.

Shook, B.A., Wasko, R.R., Rivera-Gonzalez, G.C., Salazar-Gatzimas, E., Lopez-Giraldez, F., Dash, B.C., Munoz-Rojas, A.R., Aultman, K.D., Zwick, R.K., Lei, V.*, et al.* (2018). Myofibroblast proliferation and heterogeneity are supported by macrophages during skin repair. Science *362*.

Si, Y., Tsou, C.-L., Croft, K., and Charo, I.F. (2010). CCR2 mediates hematopoietic stem and progenitor cell trafficking to sites of inflammation in mice. The Journal of clinical investigation *120*, 1192-1203.

Silva, H.M., Bafica, A., Rodrigues-Luiz, G.F., Chi, J., Santos, P.D.A., Reis, B.S., Hoytema van Konijnenburg, D.P., Crane, A., Arifa, R.D.N., Martin, P.*, et al.* (2019). Vasculature-associated fat macrophages readily adapt to inflammatory and metabolic challenges. The Journal of experimental medicine *216*, 786-806.

Sottile, V., and Seuwen, K. (2000). Bone morphogenetic protein-2 stimulates adipogenic differentiation of mesenchymal precursor cells in synergy with BRL 49653 (rosiglitazone). FEBS Lett *475*, 201-204.

Stern, J.H., Rutkowski, J.M., and Scherer, P.E. (2016). Adiponectin, Leptin, and Fatty Acids in the Maintenance of Metabolic Homeostasis through Adipose Tissue Crosstalk. Cell metabolism *23*, 770-784.

Sudo, T., Nishikawa, S., Ogawa, M., Kataoka, H., Ohno, N., Izawa, A., Hayashi, S., and Nishikawa, S. (1995). Functional hierarchy of c-kit and c-fms in intramarrow production of CFU-M. Oncogene *11*, 2469-2476.

Suganami, T., and Ogawa, Y. (2010). Adipose tissue macrophages: their role in adipose tissue remodeling. Journal of leukocyte biology *88*, 33-39.

Sullivan, T.J., Miao, Z., Zhao, B.N., Ertl, L.S., Wang, Y., Krasinski, A., Walters, M.J., Powers, J.P., Dairaghi, D.J., Baumgart, T.*, et al.* (2013). Experimental evidence for the

use of CCR2 antagonists in the treatment of type 2 diabetes. Metabolism *62*, 1623-1632.

Sun, C., Berry, W.L., and Olson, L.E. (2017). PDGFRalpha controls the balance of stromal and adipogenic cells during adipose tissue organogenesis. Development *144*, 83-94.

Surmi, B.K., and Hasty, A.H. (2008). Macrophage infiltration into adipose tissue: initiation, propagation and remodeling. Future Lipidol *3*, 545-556.

Tsou, C.L., Peters, W., Si, Y., Slaymaker, S., Aslanian, A.M., Weisberg, S.P., Mack, M., and Charo, I.F. (2007). Critical roles for CCR2 and MCP-3 in monocyte mobilization from bone marrow and recruitment to inflammatory sites. The Journal of clinical investigation *117*, 902-909.

Valdearcos, M., Douglass, J.D., Robblee, M.M., Dorfman, M.D., Stifler, D.R., Bennett, M.L., Gerritse, I., Fasnacht, R., Barres, B.A., Thaler, J.P.*, et al.* (2017). Microglial Inflammatory Signaling Orchestrates the Hypothalamic Immune Response to Dietary Excess and Mediates Obesity Susceptibility. Cell Metab *26*, 185-197 e183.

Valdearcos, M., Robblee, M.M., Benjamin, D.I., Nomura, D.K., Xu, A.W., and Koliwad, S.K. (2014). Microglia dictate the impact of saturated fat consumption on hypothalamic inflammation and neuronal function. Cell Rep *9*, 2124-2138.

Vaziri, C., and Faller, D.V. (1996). Down-regulation of platelet-derived growth factor receptor expression during terminal differentiation of 3T3-L1 pre-adipocyte fibroblasts. The Journal of biological chemistry *271*, 13642-13648.

Wei, S., Lightwood, D., Ladyman, H., Cross, S., Neale, H., Griffiths, M., Adams, R., Marshall, D., Lawson, A., McKnight, A.J.*, et al.* (2005). Modulation of CSF-1-regulated post-natal development with anti-CSF-1 antibody. Immunobiology *210*, 109-119.

Weisberg, S.P., Hunter, D., Huber, R., Lemieux, J., Slaymaker, S., Vaddi, K., Charo, I., Leibel, R.L., and Ferrante, A.W., Jr. (2006). CCR2 modulates inflammatory and metabolic effects of high-fat feeding. The Journal of clinical investigation *116*, 115-124.

Weisberg, S.P., McCann, D., Desai, M., Rosenbaum, M., Leibel, R.L., and Ferrante, A.W., Jr. (2003). Obesity is associated with macrophage accumulation in adipose tissue. J Clin Invest *112*, 1796-1808.

Wernstedt Asterholm, I., Tao, C., Morley, T.S., Wang, Q.A., Delgado-Lopez, F., Wang, Z.V., and Scherer, P.E. (2014). Adipocyte inflammation is essential for healthy adipose tissue expansion and remodeling. Cell Metab *20*, 103-118.

Wise, A. (1975). Adipocyte number and size in hypothalamic obesity induced in weanling mice by gold thioglucose and bipiperidyl mustard. Nutr Metab *19*, 291-298.

Wolf, Y., Boura-Halfon, S., Cortese, N., Haimon, Z., Sar Shalom, H., Kuperman, Y., Kalchenko, V., Brandis, A., David, E., Segal-Hayoun, Y.*, et al.* (2017). Brown-adipose-

tissue macrophages control tissue innervation and homeostatic energy expenditure. Nature immunology *18*, 665-674.

Woodcock, K.J., Kierdorf, K., Pouchelon, C.A., Vivancos, V., Dionne, M.S., and Geissmann, F. (2015). Macrophage-derived upd3 cytokine causes impaired glucose homeostasis and reduced lifespan in Drosophila fed a lipid-rich diet. Immunity *42*, 133-144.

Xu, H., Barnes, G.T., Yang, Q., Tan, G., Yang, D., Chou, C.J., Sole, J., Nichols, A., Ross, J.S., Tartaglia, L.A.*, et al.* (2003). Chronic inflammation in fat plays a crucial role in the development of obesity-related insulin resistance. J Clin Invest *112*, 1821-1830.

Zettervall, C.J., Anderl, I., Williams, M.J., Palmer, R., Kurucz, E., Ando, I., and Hultmark, D. (2004). A directed screen for genes involved in Drosophila blood cell activation. Proceedings of the National Academy of Sciences of the United States of America *101*, 14192-14197.

Zeyda, M., Gollinger, K., Kriehuber, E., Kiefer, F.W., Neuhofer, A., and Stulnig, T.M. (2010). Newly identified adipose tissue macrophage populations in obesity with distinct chemokine and chemokine receptor expression. Int J Obes (Lond) *34*, 1684-1694.

Zheng, H., Wang, X., Guo, P., Ge, W., Yan, Q., Gao, W., Xi, Y., and Yang, X. (2017). Premature remodeling of fat body and fat mobilization triggered by platelet-derived growth factor/VEGF receptor in Drosophila. FASEB J *31*, 1964-1975.

Acknowledgements. This study is dedicated to the memory of Lucile Crozet. This work was supported by NIH/NCI P30CA008748 to MSKCC, NIH/NIAID 1R01AI130345, NIH/NHLBI R01HL138090, Ludwig institute for Cancer research basic immunology grant and Cycle For Survival grants to FG. This work was also supported by Leducq transatlantic network of excellence to CKG and FG, NIH/NCI F32CA225036 to NC and Alan and Sandra Gerry Metastasis and Tumor Ecosystems Center fellowship to PLL. The authors thank John Frampton, Jeffrey Pollard, and Thomas Boehm, for providing mouse strains, Harmony Ketchum for her technical assistance with the *Csf1r*$^{-/-}$ mice, the molecular cytology core at MSKCC for help with preparation of histological samples. The authors acknowledge Maria Pokrovskii, James Muller, and all members of the Geissmann lab for helpful suggestions and editing the manuscript.

Author contribution. FG, LC, NC designed the study, analyzed data, and wrote the manuscript. LC, NC, and PLL performed and analyzed experiment in mice. NC performed *Drosophila* experiments. EM contributed to generation and analysis of *Tnfrsf11a*^{Cre}*; Csf1r*$^{f/f}$ mice. TL performed and analyzed flow-cytometry experiments. IRH, CKG analyzed RNAseq experiments and helped preparing the manuscript. PLL helped with immunofluorescence and flow cytometry analyses. RS provided Csf1r-deficient mice and intellectual input. EM present address: Developmental Biology of the Innate Immune System, LIMES Institute, University of Bonn, 53115 Bonn, Germany.

Figure Legends.

Figure 1. White adipose tissue deficiency in absence of tissue resident macrophages. (**A**) tSNE plot (**see extended methods**) and tSNE color coded flow plot representation of flow cytometry analysis of F4/80+ cells among the stromal vascular fraction from the iWAT of P26 *Csf1r*$^{f/f}$ mice (n=15), *Csf1r*^{Cre}*; Csf1r*$^{f/f}$ (n=4, from 2 litters), *Flt3*^{Cre}*; Csf1r*$^{f/f}$ (n=5, from 3 litters), *CCR2*$^{-/-}$ (n=4, from 2 litters) mice, and P7 *Tnfrsf11a*^{Cre}*;Csf1r*$^{f/f}$ (n=9, from 3 litters). Right panel represent May-Grunwald Giemsa staining of FACS-sorted macrophages populations from C57Bl/6J mice. (**B**) Gross morphology of iWAT and weights of iWAT, eWAT, and iBAT from P26 *Csf1r*^{Cre}*; Csf1r*$^{f/f}$ and control littermates (n=4-5 from 2 litters for *Csf1r*^{Cre}*; Csf1r*$^{f/f}$ mice; n=6-8, from 3 litters for *Csf1r*$^{f/f}$ mice). (**C**) Gross morphology of iWAT from P26 *Flt3*^{Cre}*; Csf1r*$^{f/f}$, *CCR2*$^{-/-}$, and control littermates (n=7-9, from 5 litters for *Flt3*^{Cre}*; Csf1r*$^{f/f}$ mice, n=3-7, from 3-4 litters for *Csf1r*$^{f/f}$ mice; n=6, from 2 litters for *CCR2*$^{-/-}$ mice, n=3, from 2 litters for *CCR2*$^{+/-}$ mice). (**D**) Gross morphology of P26 iWAT from *Tnfrsf11a*^{Cre}*; Csf1r*$^{f/f}$ (n=9, from 4 litters), *Tnfrsf11a*^{Cre}*; PU.1*$^{f/f}$ (n=5, from 3 litters), and control littermates (n=5-10, from 3-5 litters). (**E**) iWAT, eWAT, and iBAT weights from P26 *Tnfrsf11a*^{Cre}*; Csf1r*$^{f/f}$ mice and littermate controls. (**F**) Photography and H&E staining of liver from *Tnfrsf11a*^{Cre}*; Csf1r*$^{f/f}$ mice and littermate controls, at P26 (n=8-10, from 7 litters). Liver triglycerides (TG), as µg per mg of tissue at P26 (n=4, from 2 litters). (**G**) qPCR analysis (**Figure S4A**) of the indicated transcripts in total iBAT and iWAT of P26 *Tnfrsf11a*^{Cre}*; Csf1r*$^{f/f}$ and littermate control mice (n=5-10, from 4 litters). Heatmap depicts mean transcripts ($2^{-\Delta Ct}$) normalized to *Gapdh.* (**H**) Representative flow cytometry plot of iWAT from 1 month old *Csf1r*^{MeriCreMer}*;Rosa*$^{LSL-YFP}$ mice pulse labeled with 4-hydroxy tamoxifen at E8.5. (Flow plot representative of n=4, from 2 litters). Each dot represents one mouse, p values obtained by one-way ANOVA with Sidak's correction unless otherwise indicated.

Figure 2. Lipid storage by adipocytes is impaired in the absence of tissue resident macrophages. (**A**) Weight of eWAT at 7, 14, and 26 days after birth (n=4-13, from 3-7 litters). p values obtained by two-way ANOVA. (**B**) Perilipin staining on paraffin-embedded tissue sections from iWAT of 7 and 26 days old *Tnfrsf11a*^{Cre}*; Csf1r*$^{f/f}$ (n=9, from 5 litters) and littermate *Csf1r*$^{f/f}$ mice (n=10, from 5 litters). (**C**) Fluorescent whole mount images of P26 iWAT from *Tnfrsf11a*^{Cre}*; Csf1r*$^{f/f}$ and *Csf1r*$^{f/f}$ littermate control mice (n=4, from 4 litters) stained for DAPI, CD31, PDGFRa, Perilipin, Bodipy, and F4/80. (**D**) Volume distribution of iWAT adipocytes from P26 *Tnfrsf11a*^{Cre}*; Csf1r*$^{f/f}$ and littermate *Csf1r*$^{f/f}$ mice as determined from whole mount imaging as represented in **C,** n=3, from 3 litters, 100-200 adipocytes per replicate. (**E**) Quantification of PDGFRa^{+} cells from iWAT paraffin embedded tissue sections of P26 mice. Each dot represents an independent value obtained from an average count of 3 fields from a single paraffin embedded iWAT section (n=3 from 3 litters for *Csf1r*$^{f/f}$ and *Tnfrsf11a*^{Cre}*; Csf1r*$^{fl+}$, n=6 from 3 litters for *Tnfrsf11a*^{Cre}*; Csf1r*$^{f/f}$). (**F**) qPCR analysis of the indicated growth factors in total iWAT from P7 *Tnfrsf11a*^{Cre}*; Csf1r*$^{f/f}$ and littermate control mice (n=4-6, from 2-3 litters). (**G**) qPCR analysis of the indicated growth factors in FACS-sorted iWAT macrophages from 4 week old *C57Bl/6J* mice. $2^{-\Delta Ct}$ calculated relative to *Gapdh* and *ActinB.* Each dot represents one mouse (n=10-30). (**H**) Fluorescent whole mount images of P26 iWAT from *Tnfrsf11a*^{Cre}*; Csf1r*$^{f/f}$ and *Csf1r*$^{f/f}$ littermate control mice (n=5, from 4 litters) stained with F4/80 and PDGFcc antibodies and Bodipy. Quantification of proportion of PDGFcc^{+} cells that express F4/80^{+}. Each dot

represents one mouse. p values obtained by one-way ANOVA with Sidak's correction unless otherwise indicated.

Figure 3. Hemocytes control triglyceride storage by fat body cells in *Drosophila* via *PDGF/VEGF* family growth factors. (**A**) Fluorescent images of L3 larvae depicting the expression pattern of hemocyte-specific drivers Hemolectin (*Hml*) and Serpent (*Srp*) as indicated by GFP and mCherry, respectively (n=3). Whole mount image of Srp^{Hemo}-*mCherry* hemocytes in contact with GFP^{+} fat body cells in Srp^{Hemo}*-mCherry; c564-gal4>uas-GFP* L3 larvae (n=3). (**B**) Triglyceride level (TG) from L3 larvae of Srp^{Hemo}-*gal4>uas-reaper, Hml-gal4>uas-reaper,* and control larvae (n=9-11, from 4 crosses**,** 10 larvae/replicate). TG values were normalized to the total protein. p values obtained by one-way ANOVA with Sidak's correction. (**C**) Size distribution of $Bodipy^{+}$ fat body cells in wandering L3 Srp^{Hemo}*-gal4>uas-reaper* (n=6, from 3 crosses)*, Hml-gal4>uas-reaper* (n=9, from 4 crosses)*,* and control larvae (n=6, from 3 crosses)**.** 100 fat body cells were examined for each replicate. p values obtained by t-test comparing mean cell size*.* (**D**) Quantitative analysis of buoyancy in wandering L3 larvae from Srp^{Hemo}*-gal4>uas-reaper* and control lines (n=6, from 3 crosses). Each replicate includes 20 larvae. (**E**) TG level to total protein in wandering L3 larvae from flies with hemocyte-specific RNAi of the indicated growth factor (n=8-12, from 4 crosses, 10 larvae/replicate). p values obtained by one-way ANOVA with Sidak's correction. (**F**) Quantification of $Bodipy^{+}$ fat body cell size in L3 larvae (n=3-6, from 3-6 crosses, 25-50 cells/replicate). Each dot represent a single fat body cells. p values obtained by one-way ANOVA with Dunnett's correction. (**G**) Size distribution of $Bodipy^{+}$ fat body cells in L3 Srp^{Hemo}*-gal4>uas-pvf3-IR* (n=3, from 3 crosses) and control larvae (n=10, from 3 crosses). 100 fat body cells were measured for each replicate, p values obtained by t-test comparing mean cell size*.* (**H**) TG level to total protein in wandering L3 larvae from flies with fat body-specific RNAi of the Pvf receptor, Pvr (n=8-11, from 4 crosses, 10 larvae/replicate). p values obtained by t-test. (**I**) Quantitative analysis of buoyancy in wandering L3 larvae from $Pvf3^{EY09531}$ and control y^{1} w^{1118} L3 larvae (n=6, from 3 crosses). Each replicate includes 20 larvae. (**J**) Size distribution of $Bodipy^{+}$ fat body cells, p values obtained by t-test comparing mean fat body cell size (n=2-5, from 3 crosses). 100 fat body cells were examined for each replicate. (**K**) TG level in L3 larvae normalized to total protein (n=7-12, from 4 crosses, 10 larvae/replicate). p values obtained by t-test.

Figure 4. Resident adipose tissue macrophages control lipid storage by adipocytes in isolated fat-pad explants via local production of PDGF family growth factors. (**A**) Schematic depicting the isolation and *ex vivo* culture of eWAT *anlage* from 4 days old $Tnfrsf11a^{Cre}$*;* $Csf1r^{f/f}$ or littermate $Csf1r^{f/f}$ mice. GF: growth factor. (**B**) Fluorescent whole mount images of eWAT from 4-day-old $Csf1r^{f/f}$ mice (n=3). (**C,D**) Representative whole mount images of eWAT explants cultured for 10 days *ex vivo* from $Tnfrsf11a^{Cre}$*;* $Csf1r^{f/f}$ (n=10) or $Csf1r^{f/f}$ (n=15) littermate control mice. (**E**) qPCR analysis of the indicated genes in eWAT explants cultured for 10 days (n=7). $2^{-\Delta Ct}$ calculated relative to *Gapdh*, n.s. obtained by t-test. (**F**) Fluorescent whole mount images of eWAT explants from $Tnfrsf11a^{Cre}$*;* $Csf1r^{f/f}$ mice supplemented with vehicle control (PBS), PDGFcc, or IGF (n=3-5). (**G,H**) Size distribution and total area of $Bodipy^{+}$ area from $Csf1r^{fl/f}$ or $Tnfrsf11a^{Cre}$*;* $Csf1r^{f/f}$ eWAT explants with the indicated treatment (n=5-15). p values obtained by one-way ANOVA. The surface area of all bodipy+ cells (~20,000 cells) were measured in each explant to calculate the size distribution. (**I**) Fluorescent whole mount images of eWAT

explants from *Csf1r*$^{f/f}$ mice supplemented with Goat IgG or anti-PDGFcc neutralizing antibodies (n=5). qPCR analysis of the indicated genes in total eWAT explants cultured for 10 days (n=8-9). $2^{-\Delta Ct}$ calculated relative to *Gapdh*, n.s. obtained by t-test.

Figure 5. PDGFcc controls energy storage adipocytes of adult mice. (**A**) Mouse body weight over time fed the indicated diet (n=5). Mean ± SD, p values at 12 weeks of age obtained by t-test. (**B**) Weight of adipose tissues from 12 weeks old C57Bl/6J mice under the indicated diet and treatment (n=9 for 45%, 45% treated with anti-PDGFcc antibody, and 10% diet in control mice, n=4 for 10% fed mice treated with anti-PDGFcc antibody, from 2 independent experiment). p values obtained by one-way ANOVA with Sidak's correction. (**C**) Size distribution of iWAT adipocytes from anti-PDGFcc antibody treated mice and controls with the indicated diet (n=4). 100-200 adipocytes were examined for each replicate. p values are obtained by t-test comparing mean adipocyte size. (**D**) Fluorescent whole mount images of iWAT adipocytes from anti-PDGFcc antibody treated mice and controls (n=4). (**E**) C57Bl/6J mice were injected with anti-PDGFcc antibodies or goat IgG and their cumulative food intake was measured gravimetrically for 5 days over the first week of treatment (n=8). (**F**) Feces were collected from C57Bl/6J mice injected with anti-PDGFcc antibodies or goat IgG on day 6 of treatment and then subjected to bomb calorimetry to measure fecal caloric density (n=8). p values are obtained by t-test. (**G**) C57Bl/6J mice injected with anti-PDGFcc antibodies or goat IgG were single housed in a Promethion Metabolic Screening System to measure O_2 and CO_2 levels over 5 days during the first week of treatment (n=8). Analysis of covariance corrected cumulative energy expenditure of C57Bl/6J mice fed a 45% fat diet and injected with anti-PDGFcc antibodies or goat IgG over a period of 5 days during the first week of treatment (n=8). Each dot represents one mouse, p values are obtained by t-test. (**H**) Representative infrared images of C57Bl/6J mice injected with anti-PDGFcc antibodies or goat IgG on day 6 of treatment. Top 10% warmest pixels were used for the quantification of iBAT surface area temperatures. Dorsal surface area temperature was calculated using top 20% warmest pixels (n=8). p values obtained by one-way ANOVA with Sidak's correction. (**I**) qPCR analysis (**Figure S8D-F**) of indicated transcripts in iBAT, iWAT, and eWAT of 12 week old C57Bl/6J mice injected with anti-PDGFcc antibodies or goat IgG for 6 weeks (n=8). Heatmap depicts mean transcripts ($2^{-\Delta Ct}$) normalized to *Gapdh.* (**J**) Representative H&E staining of livers from mice on the indicated diet and treatment (n=4 from 2 independent experiments). (**K**) Liver Triglycerides per mg of tissue in mice on the indicated diet and treatment (n=8 for 45%, 45% treated with anti-PDGFcc antibody, and 10% diet in control mice, n=4 for 10% fed mice treated with anti-PDGFcc antibody). p values obtained by one-way ANOVA with Sidak's correction. (**L**) qPCR analysis of *Tnf* and *Il1b* transcripts in the liver of mice fed 10% or 45% fat diet with the indicated treatment, normalized to *Gapdh* ($2^{-\Delta Ct}$). Each dot represents one mouse (n=8 for 45%, 45% treated with anti-PDGFcc antibody, and 10% diet in control mice, n=4 for 10% fed mice treated with anti-PDGFcc antibody). p values obtained by one-way ANOVA with Sidak's correction.

Figure 6. Resident adipose tissue macrophages are required for adipocyte hypertrophy in obese mice. (**A**) Fluorescent whole mount image of Tim4+ macrophages surrounding adipocytes in the iWAT of lean 14 week old C57Bl/6J mice. (**B**) Representative flow plots depicting expression of Tim4, CD11c, MHCII, and forward and side size scatter (SSC and FSC) by the indicated color-coded clusters in eWAT macrophages of 14 week-old mice as determined by flow cytometry analysis (n=5). (**C**) Flow cytometry quantification of eWAT adipose tissue macrophages from *Ccr2*$^{-/-}$ mice and

and *Ccr2*$^{+/-}$ littermate controls (n=4 fed a 10% lipid diet, n=5 fed a 45% lipid diet). (**D**) Flow cytometry analysis of blood monocytes and adipose tissue macrophages from iWAT of parabiotic pairs between CD45.1 and CD45.2 females fed 10% or 45% lipid diet. 2 pairs were analyzed per group, each dot represents one mouse. (**E**) Multidimensional scaling analysis of RNA sequencing performed on adipose tissue macrophages and blood Ly6C^{hi} monocytes sorted from C57Bl/6J males fed 10%, 45%, or 45%→10% lipid diet (n=2). (**F**) Expression of indicated genes, relative to *Gapdh* and *Actinb* ($2^{-\Delta Ct}$), as determined by qPCR in FACS-sorted iWAT macrophage subsets and blood monocytes in 14-week-old C57Bl/6J fed a 10% or 45% lipid diet for 8 weeks **(**n=7 from 2 independent experiments**)**. (**G**) qPCR analysis of *Pdgfc* transcripts in total iWAT, normalized to *Gapdh* ($2^{-\Delta Ct}$). *Ccr2*$^{+/-}$ (n=6, from 2 litters), and littermate controls (n=7, from 2litters) were fed 10% or 45% diets for 8 weeks. C57Bl/6J mice were treated with PLX5622 (n=8)**,** aPDGFcc neutralizing antibodies (n=8), a-CSF1R blocking antibodies (n=5), or the appropriate controls (n=10 for 10% and n=15 for 45%) for 6 weeks on the indicated diet. (**H**) Weight of eWAT and iWAT from mice with the indicated genotypes and treatments. *Ccr2*$^{+/-}$ (n=9, from 3 litters) and littermate controls (n=8, from 3 litters) were fed 10% or 45% diets for 8 weeks. C57Bl/6J mice were treated with PLX5622 (n=11 for 45% and n=8 for 10%, from 2 experiments), a-CSF1R blocking antibodies (n=5), or the appropriate controls (n=17 for 10% and n=21 for 45%, from 4 experiments**)** for 6 weeks. (**i**) Fluorescent whole mount images of iWAT adipocytes from mice with the indicayed treatment as in **H**. (**J,K**) Size distribution of iWAT adipocytes from from the indicated mice fed 10% or 45% diet. 100-200 adipocytes per replicate, n=3, were measured. p values obtained by t-test comparing mean adipocyte size (10% v.s. 45% for *wt*, *Ccr2*$^{+/-}$*,* and *Ccr2*$^{-/-}$ mice*,* 10% + PLX5622 v.s. 10%, 45% + PLX5622 v.s. 45%, 45% + a-CSF1R v.s. 45%). (**L**) Cumulative food intake was measured gravimetrically for 5 days over the first week of treatment (n=8). (**M**) Feces were collected from 12-week-old C57Bl/6J mice fed the indicated diet and then subjected to bomb calorimetry to measure fecal caloric density (n=8). (**N**) qPCR analysis (**Figure S15**) of indicated transcripts in iBAT, iWAT, and eWAT of 14 week old C57Bl/6J mice treated with PLX5622 for 8 weeks (n=5). Heatmap depicts mean transcripts ($2^{-\Delta Ct}$) normalized to *Gapdh.* **(O)** qPCR analysis of *Pdgfc* transcripts in total iWAT (n=4), normalized to *Gapdh* ($2^{-\Delta Ct}$). (**P**) Fluorescent whole mount images of iWAT adipocytes from PLX5622-treated and control *Lepr* $^{-/-}$ mice (n=4). Size distribution of iWAT adipocytes from PLX5622-treated and control *Lepr* $^{-/-}$ mice. 100-200 adipocytes per replicate, n=4, were measured. p values obtained by t-test. Each dot represents one mouse, p values are obtained by one-way ANOVA with Sidak's correction unless otherwise stated.

FIGURE_1

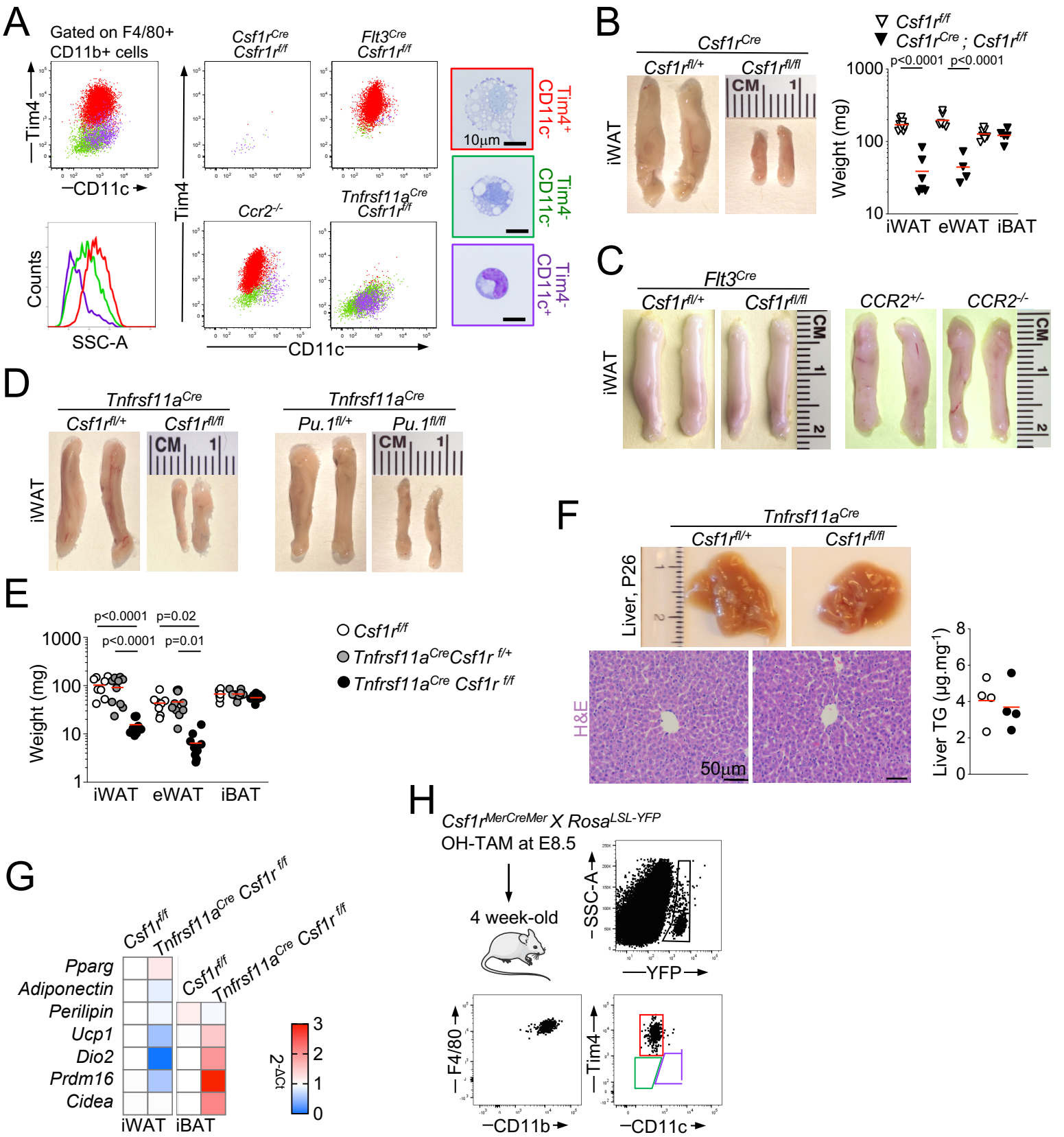

Figure 1. White adipose tissue deficiency in absence of tissue resident macrophages. (**A**) tSNE plot (**see extended methods**) and tSNE color coded flow plot representation of flow cytometry analysis of F4/80+ cells among the stromal vascular fraction from the iWAT of P26 *Csf1r*$^{f/f}$ mice (n=15), *Csf1r*^{Cre}*; Csf1r*$^{f/f}$ (n=4, from 2 litters), *Flt3*^{Cre}*; Csf1r*$^{f/f}$ (n=5, from 3 litters), *CCR2*$^{-/-}$ (n=4, from 2 litters) mice, and P7 *Tnfrsf11a*^{Cre}*;Csf1r*$^{f/f}$ (n=9, from 3 litters). Right panel represent May-Grunwald Giemsa staining of FACS-sorted macrophages populations from C57Bl/6J mice. (**B**) Gross morphology of iWAT and weights of iWAT, eWAT, and iBAT from P26 *Csf1r*^{Cre}*; Csf1r*$^{f/f}$ and control littermates (n=4-5 from 2 litters for *Csf1r*^{Cre}*; Csf1r*$^{f/f}$ mice; n=6-8, from 3 litters for *Csf1r*$^{f/f}$ mice). (**C**) Gross morphology of iWAT from P26 *Flt3*^{Cre}*; Csf1r*$^{f/f}$, *CCR2*$^{-/-}$, and control littermates (n=7-9, from 5 litters for *Flt3*^{Cre}*; Csf1r*$^{f/f}$ mice, n=3-7, from 3-4 litters for *Csf1r*$^{f/f}$ mice; n=6, from 2 litters for *CCR2*$^{-/-}$ mice, n=3, from 2 litters for *CCR2*$^{+/-}$ mice). (**D**) Gross morphology of P26 iWAT from *Tnfrsf11a*^{Cre}*; Csf1r*$^{f/f}$ (n=9, from 4 litters), *Tnfrsf11a*^{Cre}*; PU.1*$^{f/f}$ (n=5, from 3 litters), and control littermates (n=5-10, from 3-5 litters). (**E**) iWAT, eWAT, and iBAT weights from P26 *Tnfrsf11a*^{Cre}*; Csf1r*$^{f/f}$ mice and littermate controls. (**F**) Photography and H&E staining of liver from *Tnfrsf11a*^{Cre}*; Csf1r*$^{f/f}$ mice and littermate controls, at P26 (n=8-10, from 7 litters). Liver triglycerides (TG), as µg per mg of tissue at P26 (n=4, from 2 litters). (**G**) qPCR analysis (**Figure S4A**) of the indicated transcripts in total iBAT and iWAT of P26 *Tnfrsf11a*^{Cre}*; Csf1r*$^{f/f}$ and littermate control mice (n=5-10, from 4 litters). Heatmap depicts mean transcripts ($2^{-\Delta Ct}$) normalized to *Gapdh.* (**H**) Representative flow cytometry plot of iWAT from 1 month old *Csf1r*^{MeriCreMer}*;Rosa*$^{LSL-YFP}$ mice pulse labeled with 4-hydroxy tamoxifen at E8.5. (Flow plot representative of n=4, from 2 litters).
Each dot represents one mouse, p values obtained by one-way ANOVA with Sidak's correction unless otherwise indicated.

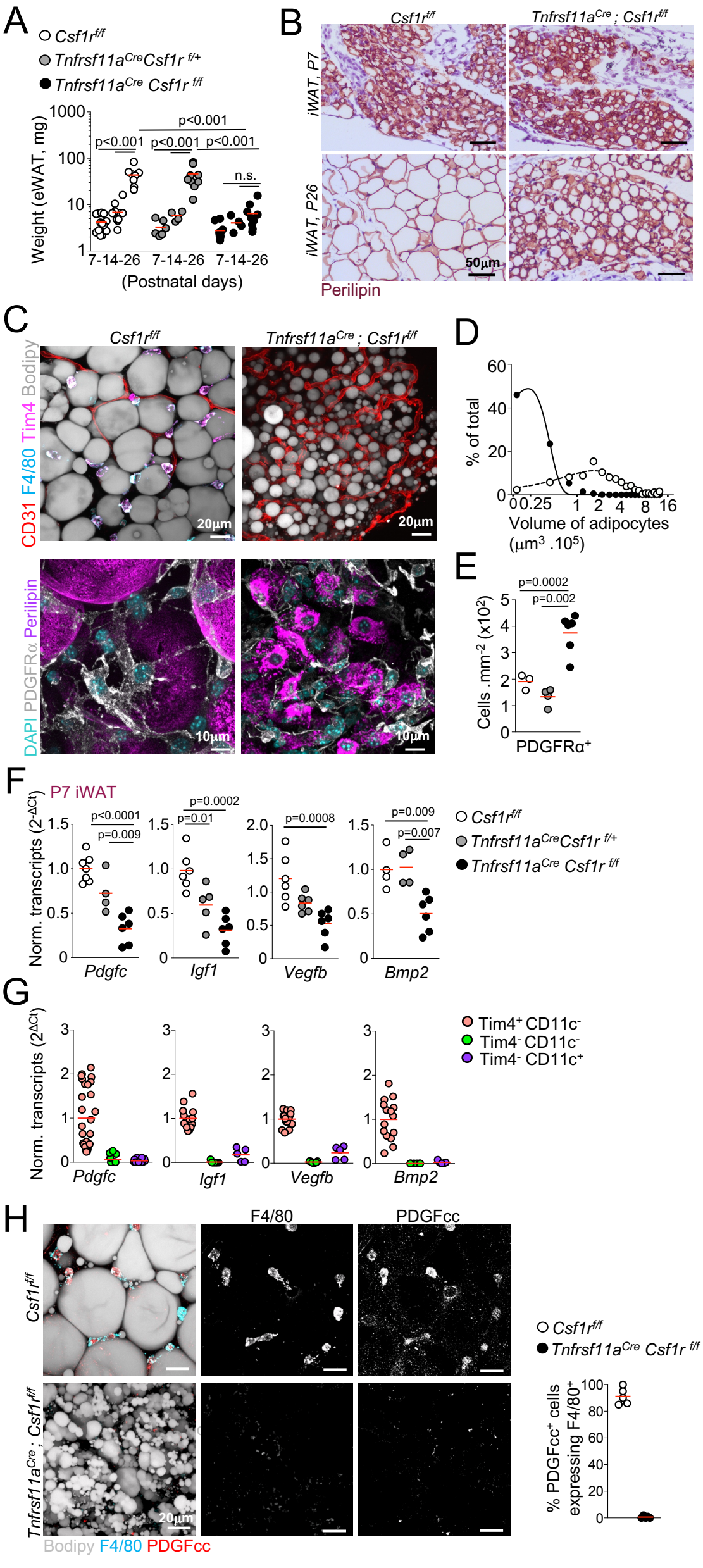

Figure 2. Lipid storage by adipocytes is impaired in the absence of tissue resident macrophages. (**A**) Weight of eWAT at 7, 14, and 26 days after birth (n=4-13, from 3-7 litters). p values obtained by two-way ANOVA. (**B**) Perilipin staining on paraffin-embedded tissue sections from iWAT of 7 and 26 days old *Tnfrsf11a^{Cre}; Csf1r$^{f/f}$* (n=9, from 5 litters) and littermate *Csf1r$^{f/f}$* mice (n=10, from 5 litters). (**C**) Fluorescent whole mount images of P26 iWAT from *Tnfrsf11a^{Cre}; Csf1r$^{f/f}$* and *Csf1r$^{f/f}$* littermate control mice (n=4, from 4 litters) stained for DAPI, CD31, PDGFRα, Perilipin, Bodipy, and F4/80. (**D**) Volume distribution of iWAT adipocytes from P26 *Tnfrsf11a^{Cre}; Csf1r$^{f/f}$* and littermate *Csf1r$^{f/f}$* mice as determined from whole mount imaging as represented in **C,** n=3, from 3 litters, 100-200 adipocytes per replicate. (**E**) Quantification of PDGFRα^{+} cells from iWAT paraffin embedded tissue sections of P26 mice. Each dot represents an independent value obtained from an average count of 3 fields from a single paraffin embedded iWAT section (n=3 from 3 litters for *Csf1r$^{f/f}$* and *Tnfrsf11a^{Cre}; Csf1r^{fl+}*, n=6 from 3 litters for *Tnfrsf11a^{Cre}; Csf1r$^{f/f}$*). (**F**) qPCR analysis of the indicated growth factors in total iWAT from P7 *Tnfrsf11a^{Cre}; Csf1r$^{f/f}$* and littermate control mice (n=4-6, from 2-3 litters). (**G**) qPCR analysis of the indicated growth factors in FACS-sorted iWAT macrophages from 4 week old *C57Bl/6J* mice. $2^{-\Delta Ct}$ calculated relative to *Gapdh* and *ActinB.* Each dot represents one mouse (n=10-30). (**H**) Fluorescent whole mount images of P26 iWAT from *Tnfrsf11a^{Cre}; Csf1r$^{f/f}$* and *Csf1r$^{f/f}$* littermate control mice (n=5, from 4 litters) stained with F4/80 and PDGFcc antibodies and Bodipy. Quantification of proportion of PDGFcc^{+} cells that express F4/80^{+}.

Each dot represents one mouse. p values obtained by one-way ANOVA with Sidak's correction unless otherwise indicated.

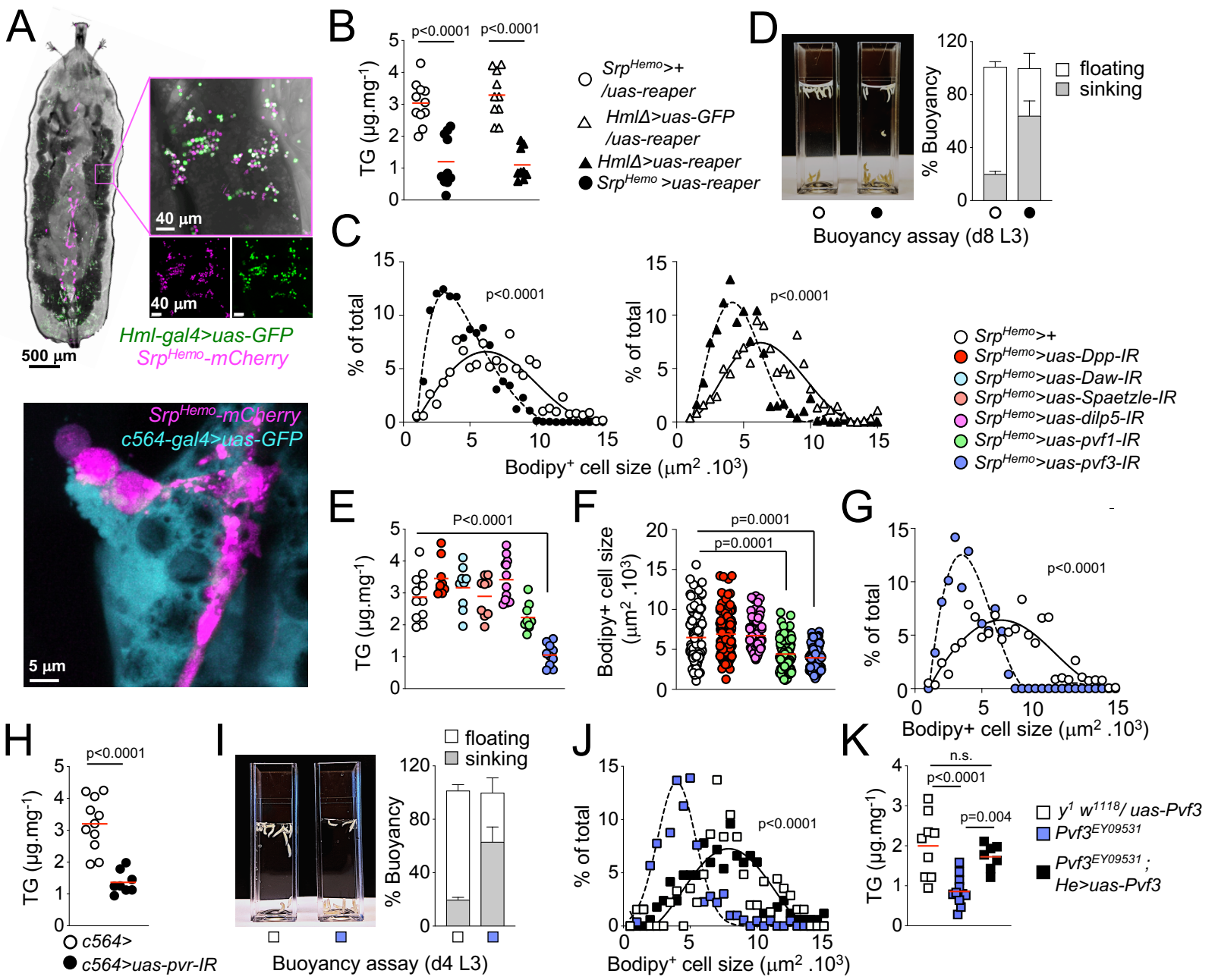

Figure 3. Hemocytes control triglyceride storage by fat body cells in *Drosophila* via *PDGF/VEGF* family growth factors. (**A**) Fluorescent images of L3 larvae depicting the expression pattern of hemocyte-specific drivers Hemolectin (*Hml*) and Serpent (*Srp*) as indicated by GFP and mCherry, respectively (n=3). Whole mount image of *Srp^{Hemo}-mCherry* hemocytes in contact with GFP^{+} fat body cells in *Srp^{Hemo}-mCherry; c564-gal4>uas-GFP* L3 larvae (n=3). (**B**) Triglyceride level (TG) from L3 larvae of *Srp^{Hemo}-gal4>uas-reaper, Hml-gal4>uas-reaper,* and control larvae (n=9-11, from 4 crosses**,** 10 larvae/replicate). TG values were normalized to the total protein. p values obtained by one-way ANOVA with Sidak's correction. (**C**) Size distribution of Bodipy^{+} fat body cells in wandering L3 *Srp^{Hemo}-gal4>uas-reaper* (n=6, from 3 crosses)*, Hml-gal4>uas-reaper* (n=9, from 4 crosses)*,* and control larvae (n=6, from 3 crosses)**.** 100 fat body cells were examined for each replicate. p values obtained by t-test comparing mean cell size*.* (**D**) Quantitative analysis of buoyancy in wandering L3 larvae from *Srp^{Hemo}-gal4>uas-reaper* and control lines (n=6, from 3 crosses). Each replicate includes 20 larvae. (**E**) TG level to total protein in wandering L3 larvae from flies with hemocyte-specific RNAi of the indicated growth factor (n=8-12, from 4 crosses, 10 larvae/replicate). p values obtained by one-way ANOVA with Sidak's correction. (**F**) Quantification of Bodipy^{+} fat body cell size in L3 larvae (n=3-6, from 3-6 crosses, 25-50 cells/replicate). Each dot represent a single fat body cells. p values obtained by one-way ANOVA with Dunnett's correction. (**G**) Size distribution of Bodipy^{+} fat body cells in L3 *Srp^{Hemo}-gal4>uas-pvf3-IR* (n=3, from 3 crosses) and control larvae (n=10, from 3 crosses). 100 fat body cells were measured for each replicate, p values obtained by t-test comparing mean cell size*.* (**H**) TG level to total protein in wandering L3 larvae from flies with fat body-specific RNAi of the Pvf receptor, Pvr (n=8-11, from 4 crosses, 10 larvae/replicate). p values obtained by t-test. (**I**) Quantitative analysis of buoyancy in wandering L3 larvae from *Pvf3^{EY09531}* and control *y^{1} w^{1118}* L3 larvae (n=6, from 3 crosses). Each replicate includes 20 larvae. (**J**) Size distribution of Bodipy^{+} fat body cells, p values obtained by t-test comparing mean fat body cell size (n=2-5, from 3 crosses). 100 fat body cells were examined for each replicate. (**K**) TG level in L3 larvae normalized to total protein (n=7-12, from 4 crosses, 10 larvae/replicate). p values obtained by t-test.

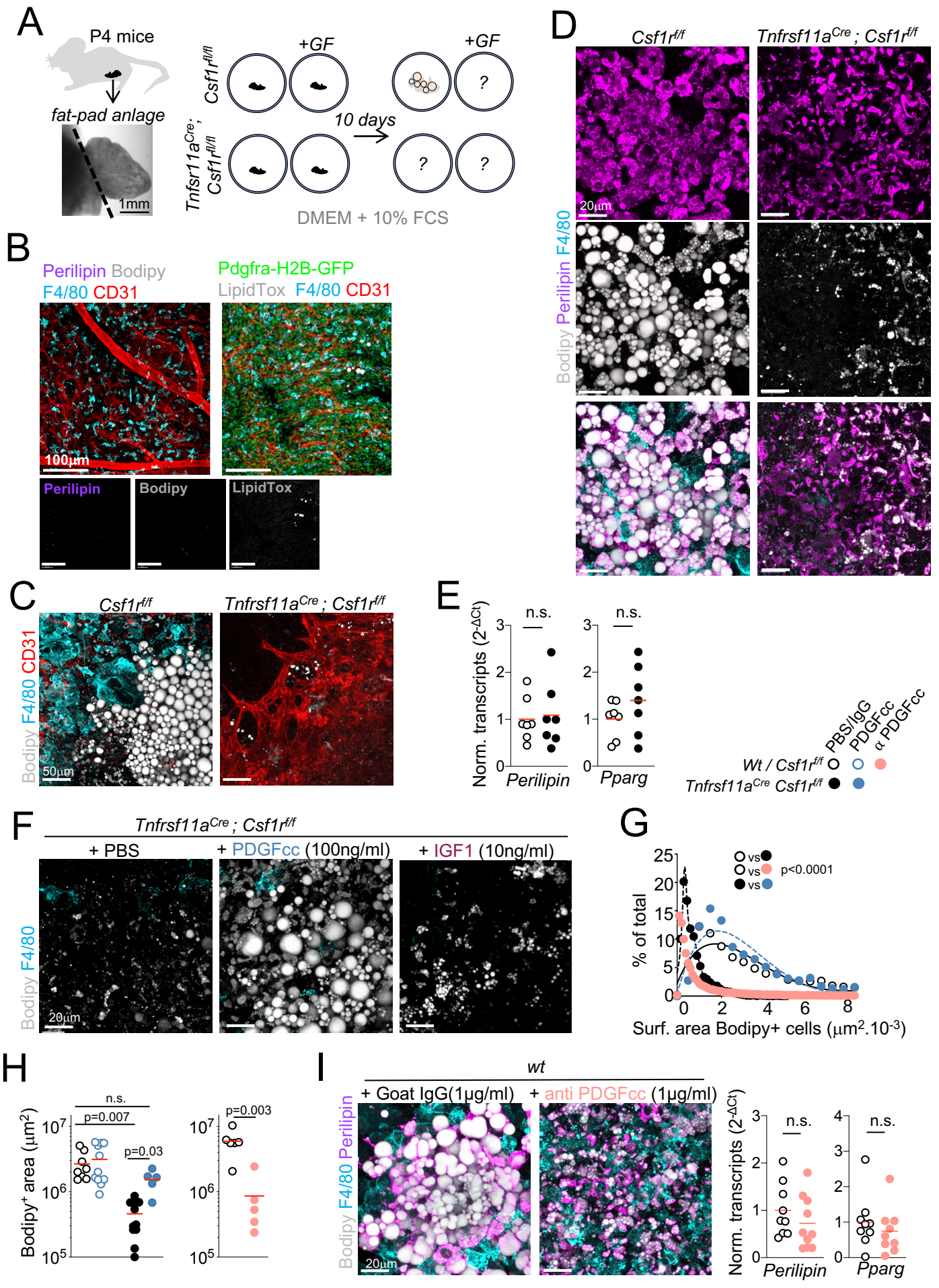

Figure 4. Resident adipose tissue macrophages control lipid storage by adipocytes in isolated fat-pad explants via local production of PDGF family growth factors. (**A**) Schematic depicting the isolation and *ex vivo* culture of eWAT *anlage* from 4 days old *Tnfrsf11a*^{Cre}*; Csf1r*$^{f/f}$ or littermate *Csf1r*$^{f/f}$ mice. GF: growth factor. (**B**) Fluorescent whole mount images of eWAT from 4-day-old *Csf1r*$^{f/f}$ mice (n=3). (**C,D**) Representative whole mount images of eWAT explants cultured for 10 days *ex vivo* from *Tnfrsf11a*^{Cre}*; Csf1r*$^{f/f}$ (n=10) or *Csf1r*$^{f/f}$ (n=15) littermate control mice. (**E**) qPCR analysis of the indicated genes in eWAT explants cultured for 10 days (n=7). $2^{-\Delta Ct}$ calculated relative to *Gapdh*, n.s. obtained by t-test. (**F**) Fluorescent whole mount images of eWAT explants from *Tnfrsf11a*^{Cre}*; Csf1r*$^{f/f}$ mice supplemented with vehicle control (PBS), PDGFcc, or IGF (n=3-5). (**G,H**) Size distribution and total area of Bodipy^{+} area from *Csf1r*$^{fl/f}$ or *Tnfrsf11a*^{Cre}*; Csf1r*$^{f/f}$ eWAT explants with the indicated treatment (n=5-15). p values obtained by one-way ANOVA. The surface area of all bodipy+ cells (~20,000 cells) were measured in each explant to calculate the size distribution. (**I**) Fluorescent whole mount images of eWAT explants from *Csf1r*$^{f/f}$ mice supplemented with Goat IgG or anti-PDGFcc neutralizing antibodies (n=5). qPCR analysis of the indicated genes in total eWAT explants cultured for 10 days (n=8-9). $2^{-\Delta Ct}$ calculated relative to *Gapdh*, n.s. obtained by t-test.

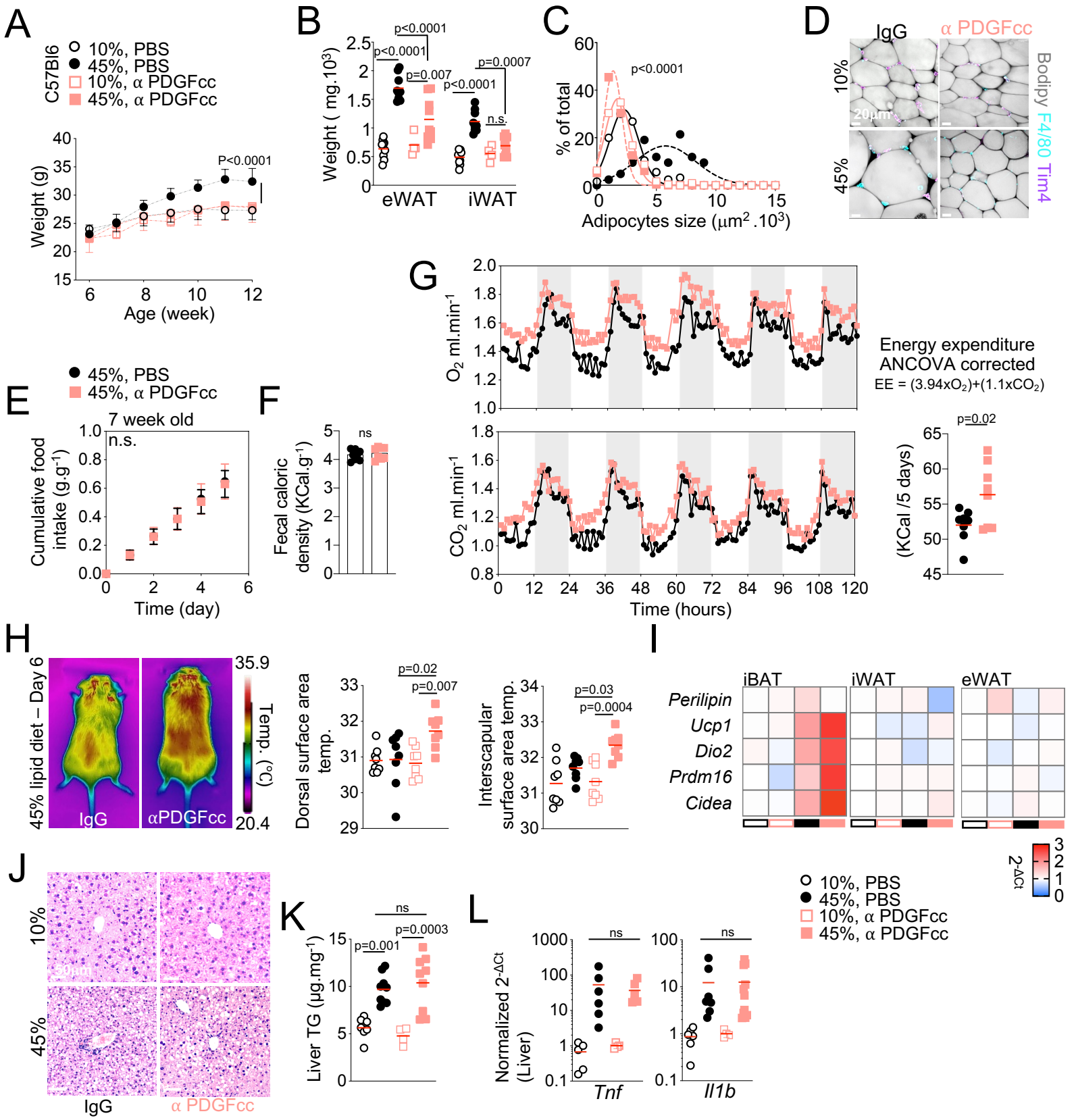

Figure 5. PDGFcc controls energy storage adipocytes of adult mice. (**A**) Mouse body weight over time fed the indicated diet (n=5). Mean ± SD, p values at 12 weeks of age obtained by t-test. (**B**) Weight of adipose tissues from 12 weeks old C57Bl/6J mice under the indicated diet and treatment (n=9 for 45%, 45% treated with anti-PDGFcc antibody, and 10% diet in control mice, n=4 for 10% fed mice treated with anti-PDGFcc antibody, from 2 independent experiment). p values obtained by one-way ANOVA with Sidak's correction. (**C**) Size distribution of iWAT adipocytes from anti-PDGFcc antibody treated mice and controls with the indicated diet (n=4). 100-200 adipocytes were examined for each replicate. p values are obtained by t-test comparing mean adipocyte size. (**D**) Fluorescent whole mount images of iWAT adipocytes from anti-PDGFcc antibody treated mice and controls (n=4). (**E**) C57Bl/6J mice were injected with anti-PDGFcc antibodies or goat IgG and their cumulative food intake was measured gravimetrically for 5 days over the first week of treatment (n=8). (**F**) Feces were collected from C57Bl/6J mice injected with anti-PDGFcc antibodies or goat IgG on day 6 of treatment and then subjected to bomb calorimetry to measure fecal caloric density (n=8). p values are obtained by t-test. (**G**) C57Bl/6J mice injected with anti-PDGFcc antibodies or goat IgG were single housed in a Promethion Metabolic Screening System to measure O_2 and CO_2 levels over 5 days during the first week of treatment (n=8). Analysis of covariance corrected cumulative energy expenditure of C57Bl/6J mice fed a 45% fat diet and injected with anti-PDGFcc antibodies or goat IgG over a period of 5 days during the first week of treatment (n=8). Each dot represents one mouse, p values are obtained by t-test. (**H**) Representative infrared images of C57Bl/6J mice injected with anti-PDGFcc antibodies or goat IgG on day 6 of treatment. Top 10% warmest pixels were used for the quantification of iBAT surface area temperatures. Dorsal surface area temperature was calculated using top 20% warmest pixels (n=8). p values obtained by one-way ANOVA with Sidak's correction. (**I**) qPCR analysis (**Figure S8D-F**) of indicated transcripts in iBAT, iWAT, and eWAT of 12 week old C57Bl/6J mice injected with anti-PDGFcc antibodies or goat IgG for 6 weeks (n=8). Heatmap depicts mean transcripts ($2^{-\Delta Ct}$) normalized to *Gapdh.* (**J**) Representative H&E staining of livers from mice on the indicated diet and treatment (n=4 from 2 independent experiments). (**K**) Liver Triglycerides per mg of tissue in mice on the indicated diet and treatment (n=8 for 45%, 45% treated with anti-PDGFcc antibody, and 10% diet in control mice, n=4 for 10% fed mice treated with anti-PDGFcc antibody). p values obtained by one-way ANOVA with Sidak's correction. (**L**) qPCR analysis of *Tnf* and *Il1b* transcripts in the liver of mice fed 10% or 45% fat diet with the indicated treatment, normalized to *Gapdh* ($2^{-\Delta Ct}$). Each dot represents one mouse (n=8 for 45%, 45% treated with anti-PDGFcc antibody, and 10% diet in control mice, n=4 for 10% fed mice treated with anti-PDGFcc antibody). p values obtained by one-way ANOVA with Sidak's correction.

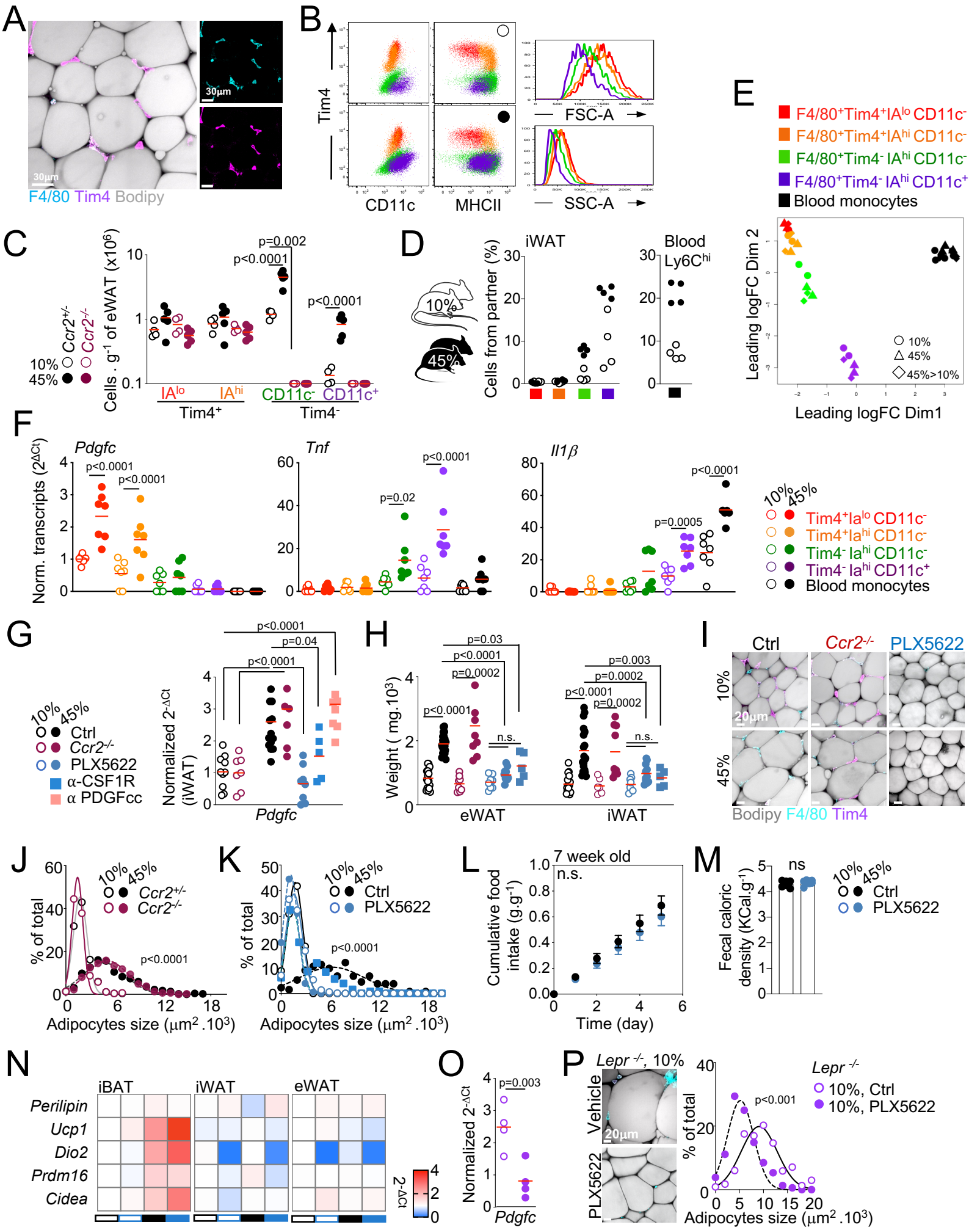

Figure 6. Resident adipose tissue macrophages are required for adipocyte hypertrophy in obese mice. (**A**) Fluorescent whole mount image of Tim4+ macrophages surrounding adipocytes in the iWAT of lean 14 week old C57Bl/6J mice. (**B**) Representative flow plots depicting expression of Tim4, CD11c, MHCII, and forward and side size scatter (SSC and FSC) by the indicated color-coded clusters in eWAT macrophages of 14 week-old mice as determined by flow cytometry analysis (n=5). (**C**) Flow cytometry quantification of eWAT adipose tissue macrophages from *Ccr2*$^{-/-}$ mice and and *Ccr2*$^{+/-}$ littermate controls (n=4 fed a 10% lipid diet, n=5 fed a 45% lipid diet). (**D**) Flow cytometry analysis of blood monocytes and adipose tissue macrophages from iWAT of parabiotic pairs between CD45.1 and CD45.2 females fed 10% or 45% lipid diet. 2 pairs were analyzed per group, each dot represents one mouse. (**E**) Multidimensional scaling analysis of RNA sequencing performed on adipose tissue macrophages and blood Ly6C^{hi} monocytes sorted from C57Bl/6J males fed 10%, 45%, or 45%→10% lipid diet (n=2). (**F**) Expression of indicated genes, relative to *Gapdh* and *Actinb* ($2^{-\Delta Ct}$), as determined by qPCR in FACS-sorted iWAT macrophage subsets and blood monocytes in 14-week-old C57Bl/6J fed a 10% or 45% lipid diet for 8 weeks **(**n=7 from 2 independent experiments**)**. (**G**) qPCR analysis of *Pdgfc* transcripts in total iWAT, normalized to *Gapdh* ($2^{-\Delta Ct}$). *Ccr2*$^{+/-}$ (n=6, from 2 litters), and littermate controls (n=7, from 2litters) were fed 10% or 45% diets for 8 weeks. C57Bl/6J mice were treated with PLX5622 (n=8)**,** αPDGFcc neutralizing antibodies (n=8), α–CSF1R blocking antibodies (n=5), or the appropriate controls (n=10 for 10% and n=15 for 45%) for 6 weeks on the indicated diet. (**H**) Weight of eWAT and iWAT from mice with the indicated genotypes and treatments. *Ccr2*$^{+/-}$ (n=9, from 3 litters) and littermate controls (n=8, from 3 litters) were fed 10% or 45% diets for 8 weeks. C57Bl/6J mice were treated with PLX5622 (n=11 for 45% and n=8 for 10%, from 2 experiments), α–CSF1R blocking antibodies (n=5), or the appropriate controls (n=17 for 10% and n=21 for 45%, from 4 experiments**)** for 6 weeks. (**i**) Fluorescent whole mount images of iWAT adipocytes from mice with the indicayed treatment as in **H**. (**J,K**) Size distribution of iWAT adipocytes from from the indicated mice fed 10% or 45% diet. 100-200 adipocytes per replicate, n=3, were measured. p values obtained by t-test comparing mean adipocyte size (10% v.s. 45% for *wt*, *Ccr2*$^{+/-}$, and *Ccr2*$^{-/-}$ mice, 10% + PLX5622 v.s. 10%, 45% + PLX5622 v.s. 45%, 45% + α-CSF1R v.s. 45%). (**L**) Cumulative food intake was measured gravimetrically for 5 days over the first week of treatment (n=8). (**M**) Feces were collected from 12-week-old C57Bl/6J mice fed the indicated diet and then subjected to bomb calorimetry to measure fecal caloric density (n=8). (**N**) qPCR analysis (**Figure S15**) of indicated transcripts in iBAT, iWAT, and eWAT of 14 week old C57Bl/6J mice treated with PLX5622 for 8 weeks (n=5). Heatmap depicts mean transcripts ($2^{-\Delta Ct}$) normalized to *Gapdh.* **(O)** qPCR analysis of *Pdgfc* transcripts in total iWAT (n=4), normalized to *Gapdh* ($2^{-\Delta Ct}$). (**P**) Fluorescent whole mount images of iWAT adipocytes from PLX5622-treated and control *Lepr* $^{-/-}$ mice (n=4). Size distribution of iWAT adipocytes from PLX5622-treated and control *Lepr* $^{-/-}$ mice. 100-200 adipocytes per replicate, n=4, were measured. p values obtained by t-test.
Each dot represents one mouse, p values are obtained by one-way ANOVA with Sidak's correction unless otherwise stated.

Fig. S1

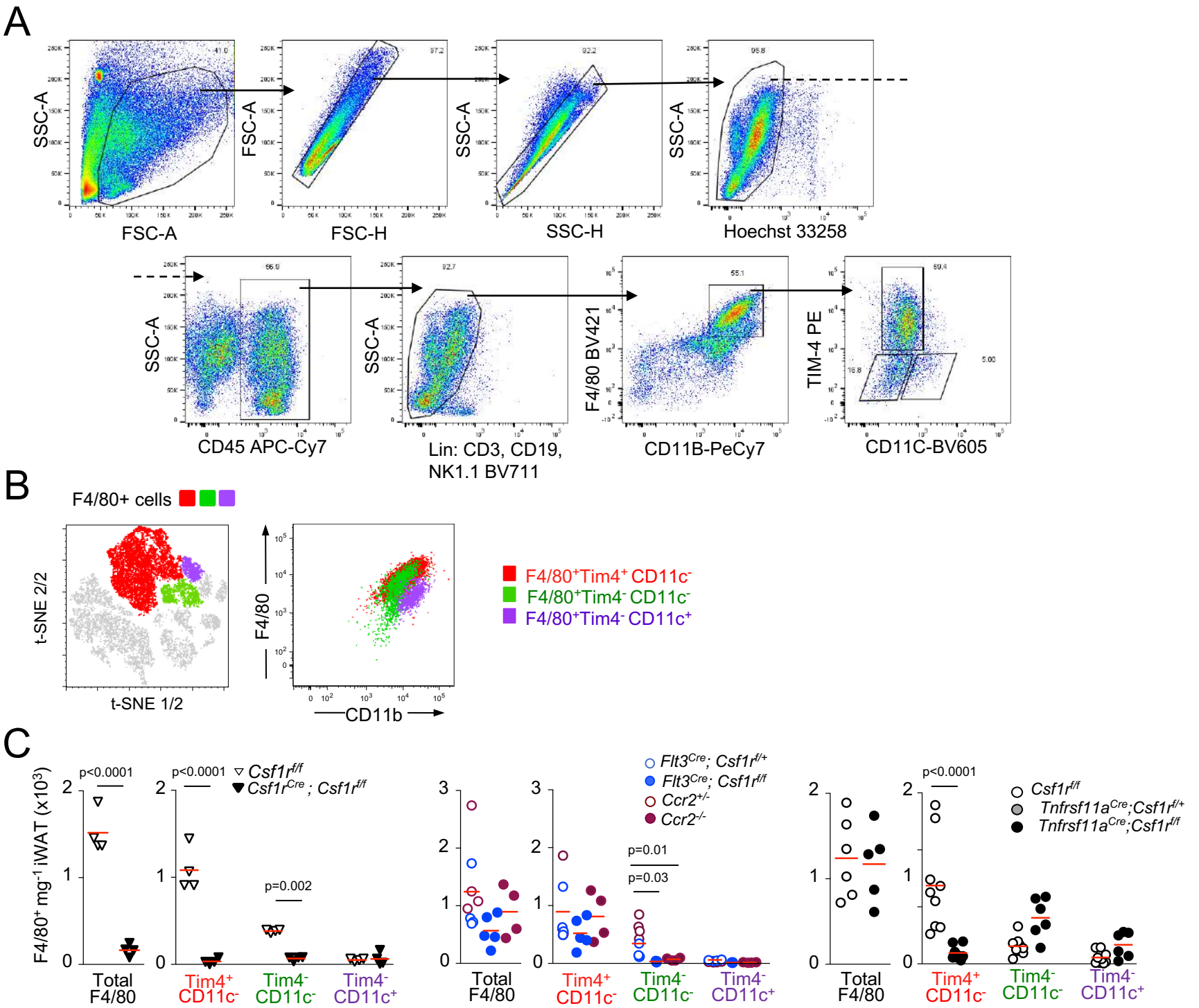

Gating strategy of *Csf1r*$^{-/-}$, *Csf1r*^{Cre}; *Csf1r*$^{f/f}$, *Flt3*^{Cre}; *Csf1r*$^{f/f}$, and *Ccr2* $^{-/-}$ mice. (**A**) Gating strategy used for flow analysis and flow sorting of different macrophage populations in the adipose tissues studied, the eWAT is represented here (representative of n=15). The same gating was used in iWAT and mWAT. Lineage is CD3, CD19, NKp46, and SiglecF. (**B**) tSNE plot (**see STAR methods**) and tSNE color coded flow plot representation of flow cytometry analysis of F4/80+ cells among the stromal vascular fraction from the iWAT of P26 *Csf1r*$^{f/f}$ mice (a, controls, n=15). (**C**) Flow cytometry quantification of adipose tissue F4/80+ macrophages gated as in **A** in P26 iWAT of *Csf1r*^{Cre}; *Csf1r*$^{f/f}$ (n=4, from 2 litters), *Flt3*^{Cre}; *Csf1r*$^{f/f}$ (n=5, from 3 litters), *CCR2*$^{-/-}$ (n=4, from 2 litters), and their littermate controls (n=4-5, from 2-3 litters). Flow cytometry quantification of adipose tissue F4/80+ macrophages from P7 iWAT of *Tnfrsf11a*^{Cre}; *Csf1r*^{ff} (n=6 from 3 litters) mice and littermate controls (n=9 from 3 litters). p values for total F4/80+ cell count was obtained by t-test.

Fig. S2

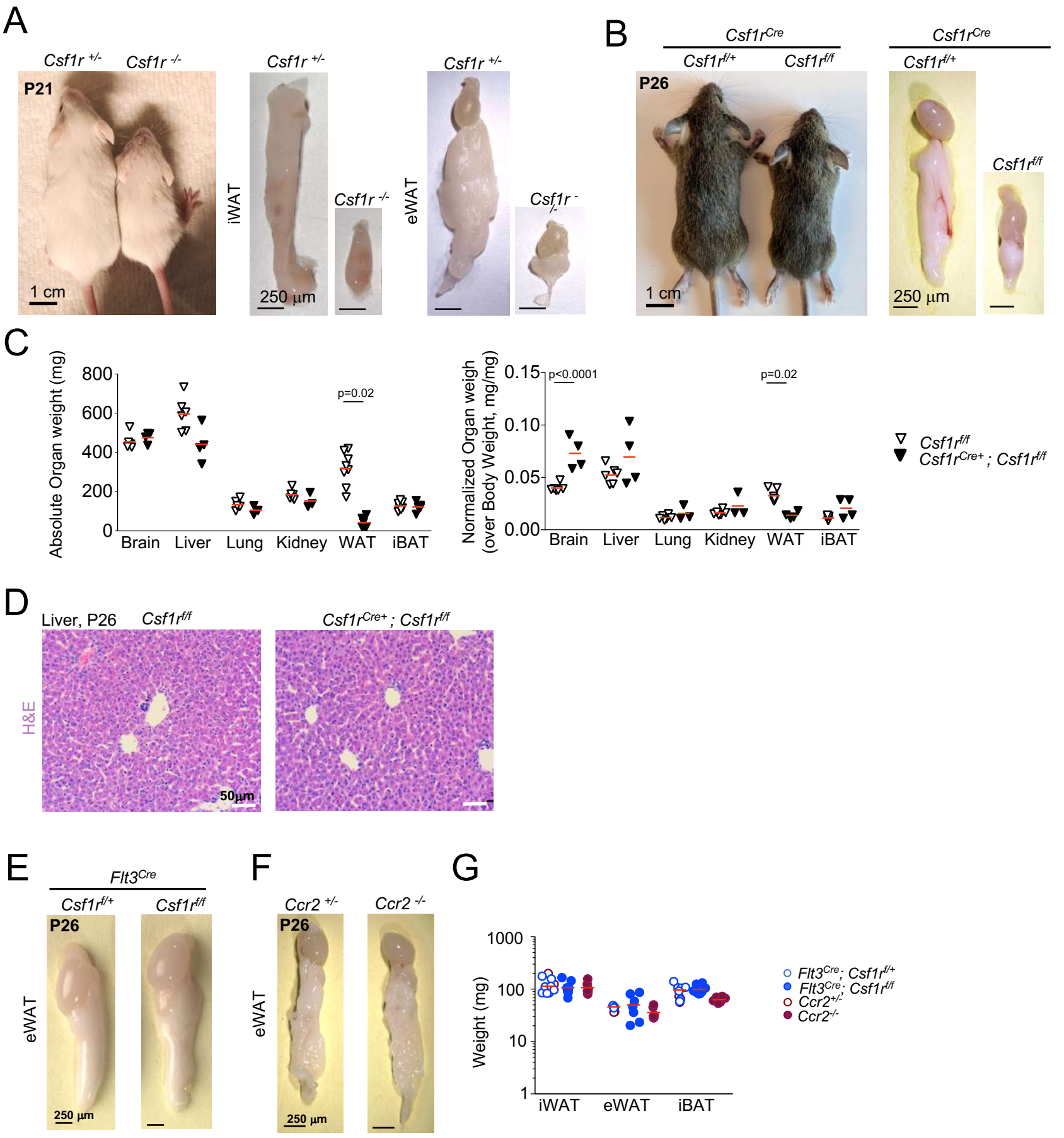

Phenotypic analysis of *Csf1r*$^{-/-}$, *Csf1r*^{Cre}; *Csf1r*$^{f/f}$, *Flt3*^{Cre}; *Csf1r*$^{f/f}$, and *Ccr2* $^{-/-}$ mice. (**A,B**) Photographs of whole mice and eWAT from *Csf1r* mutant mice (n=3, from 3 litters), *Csf1r*^{Cre};*Csf1r*$^{f/f}$ mice (n=4, from 2 litters), and control littermates (n=3-4, from 2-3 litters) at P26. (**C**) Absolute weight (left graph) and relative weight normalized to body weight (right graph) of brain, liver, lungs, kidney, WAT (eWAT, iWAT and mWAT) and iBAT from *Csf1r*^{Cre};*Csf1r*$^{f/f}$ mice (n=4, from 3 litters) and control littermates (n=6-8, from 4 litters) at P26. (**D**) H&E staining of livers from *Csf1r*^{Cre};*Csf1r*$^{f/f}$ mice (n=4, from 2 litters) and control littermates (n=4, from 2 litters) at P26. (**E,F**) Representative images of eWAT from *Flt3*^{Cre};*Csf1r*$^{f/f}$ (n=5, from 3 litters) , *Ccr2* $^{-/-}$ (n=4, from 2 litters), and their littermate controls at P26. (**G**) Weights of iWAT, eWAT, and iBAT from P26 *Flt3*^{Cre}; *Csf1r*$^{f/f}$, *CCR2*$^{-/-}$, and control littermates (n=7-9, from 5 litters for *Flt3*^{Cre}; *Csf1r*$^{f/f}$ mice, n=3-7, from 3-4 litters for *Csf1r*$^{f/f}$ mice; n=6, from 2 litters for *CCR2*$^{-/-}$ mice, n=3, from 2 litters for *CCR2*$^{+/-}$ mice).
Each dot represents one mouse, p values obtained by one-way ANOVA with Sidak's correction.

Fig. S3

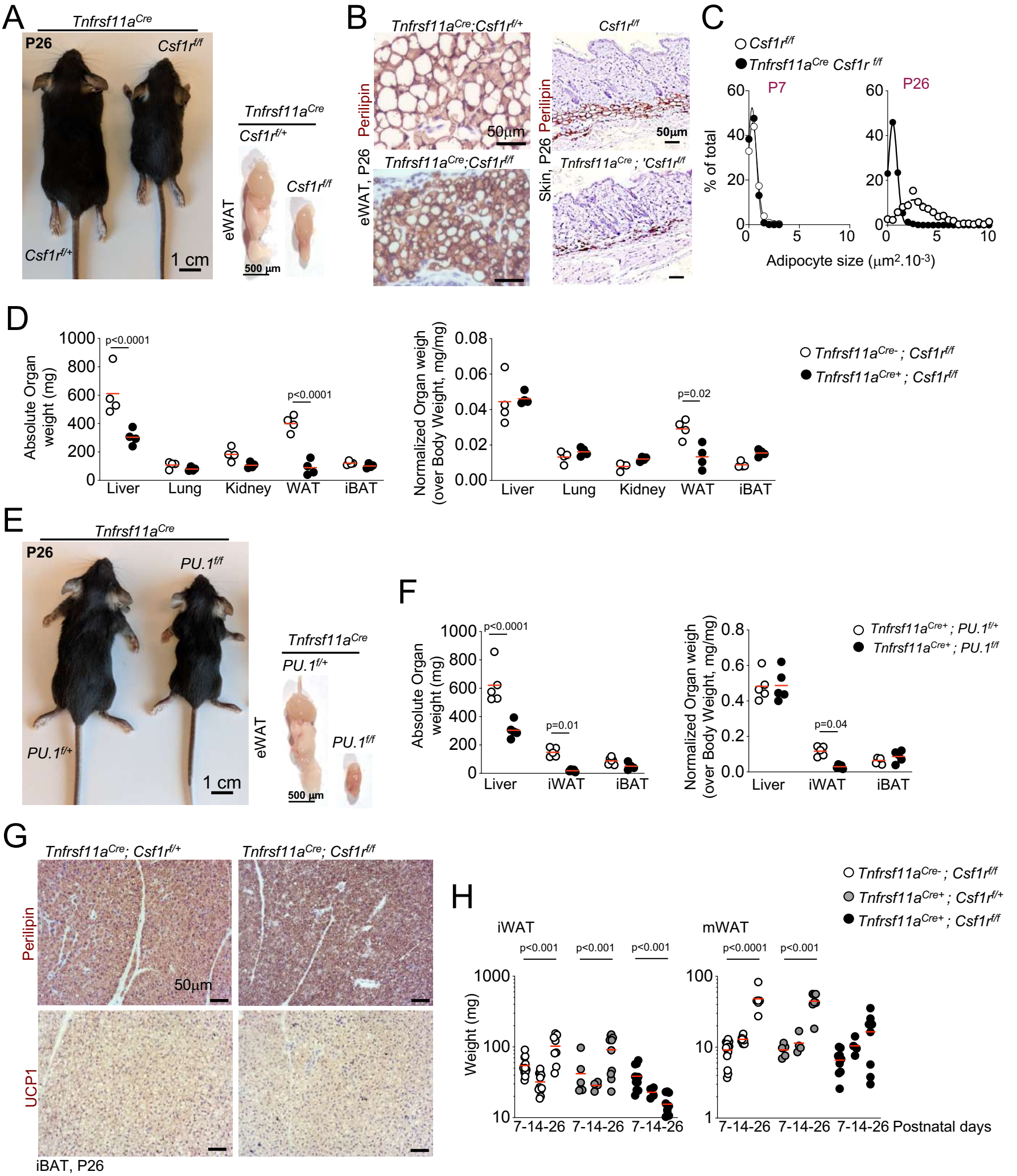

Characterization of *Tnfrsf11a^Cre;Csf1r^f/f*, *Tnfrsf11a^Cre;PU.1^f/f* mice, and littermate controls. (**A**) Photographs of whole mice and eWAT, from *Tnfrsf11a^Cre ; Csf1r^f/f* mice (n=9, from 5 litters) and control littermates (n=13, from 5 litters) at P26. (**B**) Perilipin staining of paraffin embedded eWAT and skin sections from *Tnfrsf11a^Cre; Csf1r^f/f* (n=9, from 4 litters) and littermate control (n=10, from 4 litters**)** mice at P26. (**C**) Surface area distribution of iWAT adipocytes from 7 and 26 days old *Tnfrsf11a^Cre; Csf1r^f/f* and littermate *Csf1r^f/f* mice as determined from perilipin stained paraffin-embedded tissue sections (n=3, 3 litters, 100-200 adipocytes per replicate). (**D**) Absolute weight (left graph) and relative weight normalized to body weight (right graph) of liver, lungs, kidney, WAT (eWAT, iWAT and mWAT) and iBAT from *Tnfrsf11a^Cre; Csf1r^f/f* mice (n=4, from 3 litters) and control littermates (n=4, from 3 litters) at P26. (**E**) Photographs of whole mice and eWAT from *Tnfrsf11a^Cre ; Pu.1 ^f/f* mice (n=5, from 3 litters) and control littermates (n=5, from 3 litters) at P26. (**F**) Absolute weight (left graph) and relative weight normalized to body weight (right graph) of liver, iWAT and iBAT from *Tnfrsf11a^Cre; Pu.1^f/f* mice (n=5, from 3 litters) and control littermates (n=5, from 3 litters) at P26. (**G**) Perilipin and UCP1 staining of paraffin embedded iBAT. (**H**) Weight of iWAT and mWAT in*Tnfrsf11a^Cre;Csf1r^f/f* and littermates at P7, P14 and P26 (n=4-13, from 3-8 litters). Scale bars represent indicated indicated value.
Each dot represents one mouse. p values obtained by one-way ANOVA with Sidak's correction unless otherwise indicated.

Fig. S4

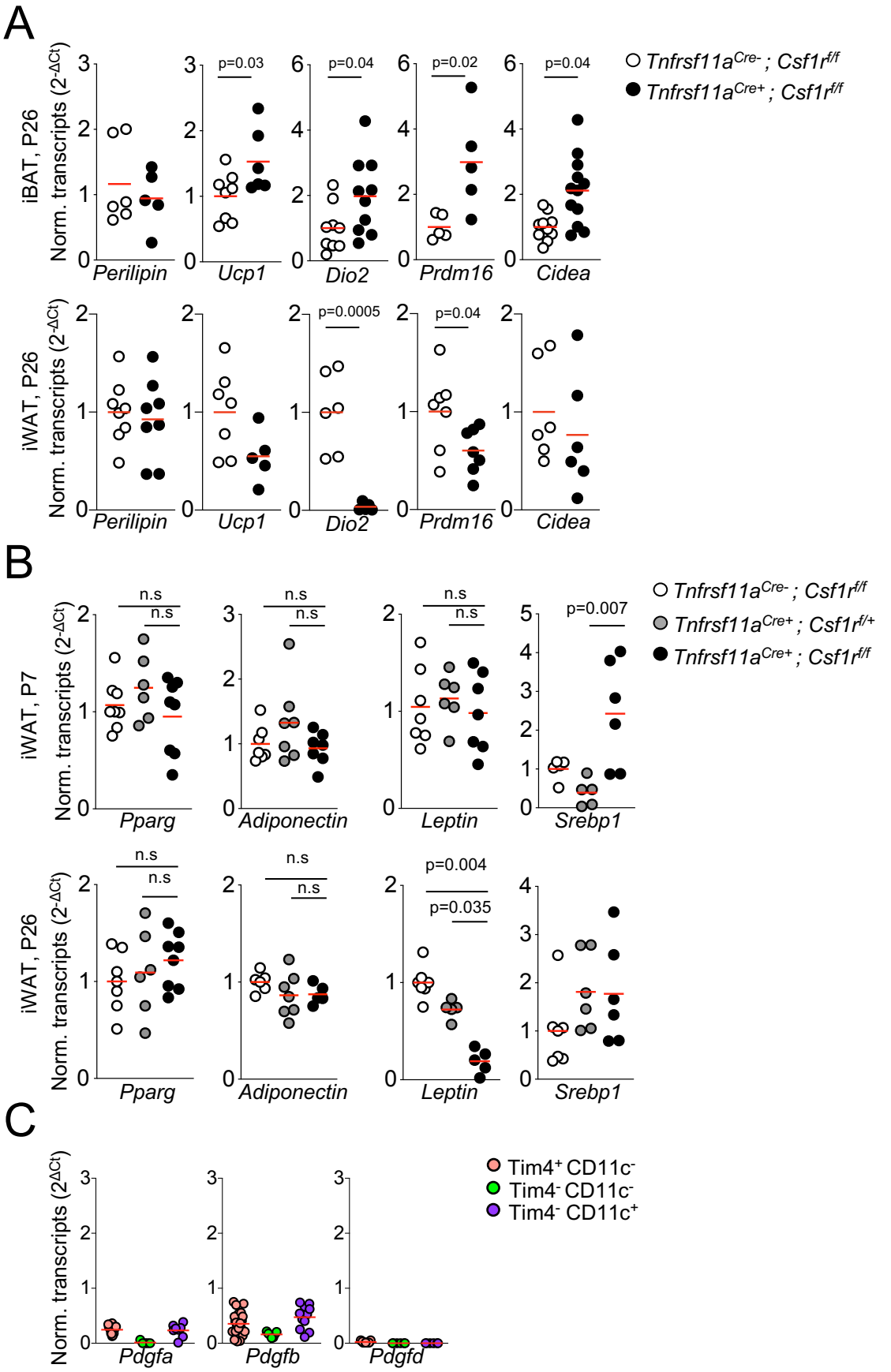

qPCR analysis of of *Tnfrsf11a^{Cre};Csf1r$^{f/f}$* and littermate controls. (**A**) qPCR analysis of *the indicated* transcripts normalized to *Gapdh* from iBAT and iWAT of *Tnfrsf11a^{Cre}; Csf1r$^{f/f}$* (n=4-12, from 4 litters) and littermate control mice (n=6-12, from 4 litters) at P26. Each dot represents one mouse, p value obtained by t-test. (**B**) qPCR analysis of the indicated genes in total iWAT from P7 or P26 *Tnfrsf11a^{Cre}; Csf1r$^{f/f}$* and littermate control mice (n=6-8, from 4 litters). Each dot represents one mouse, p values obtained by one-way ANOVA. (**C**) qPCR analysis of the indicated growth factors in FACS-sorted iWAT macrophages from 4 week old *C57Bl/6J* mice. $2^{-\Delta Ct}$ calculated relative to *Gapdh* and *ActinB*. Each dot represents one mouse (n=10-30).

Fig. S5

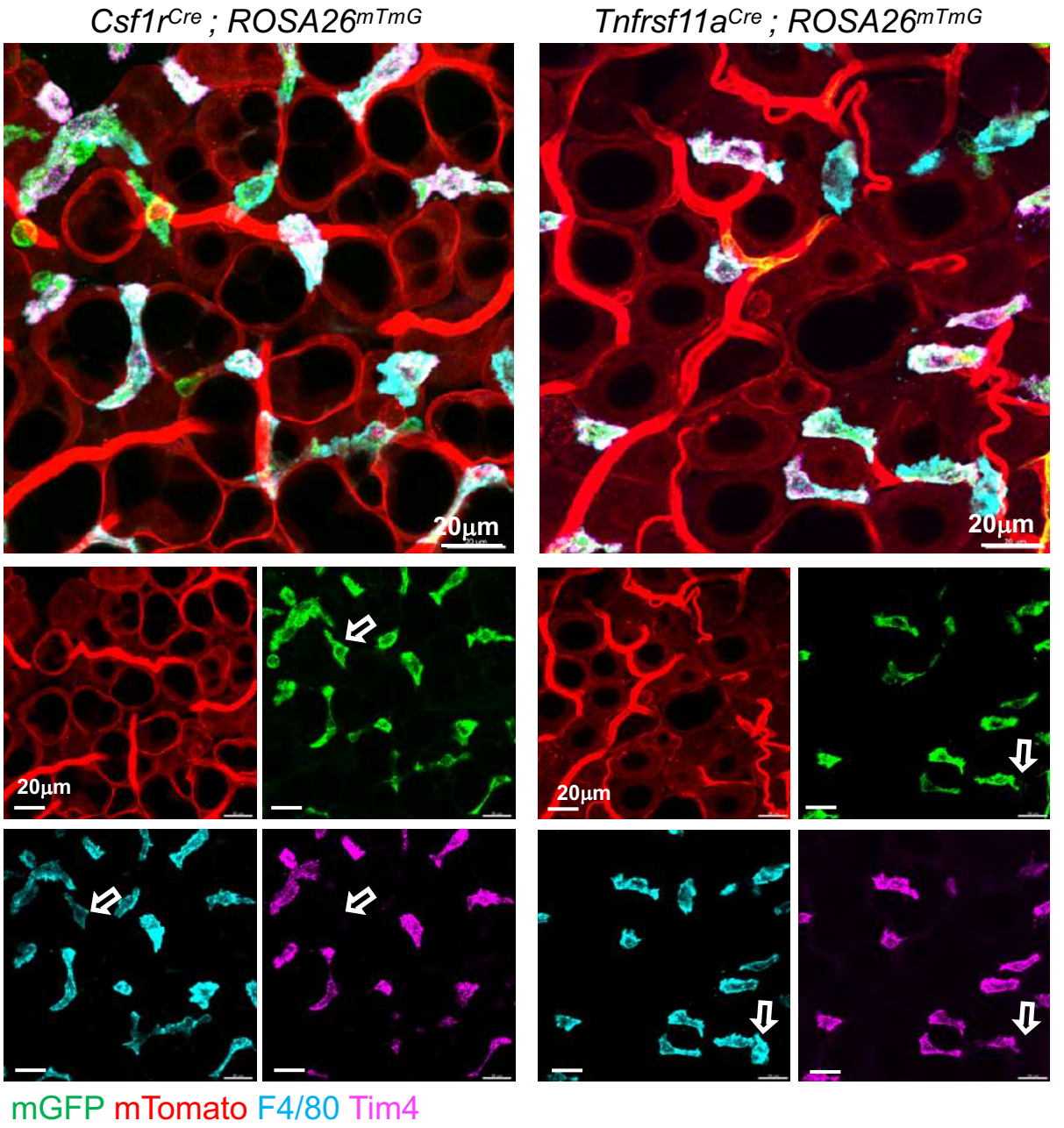

Fluorescent reporter expression in *Csf1r^{Cre}; mTmG* and *Tnfrsf11a^{Cre}; mTmG* mice. Whole mount images of 1 month old iWAT from *Csf1r^{Cre}; mTmG* and *Tnfrsf11a^{Cre}; mTmG* mice (n=3, from 2 litters). Arrow points to a F4/80^{+} Tim4^{-} macrophage. Scale bars represent 20μm.

Fig. S6

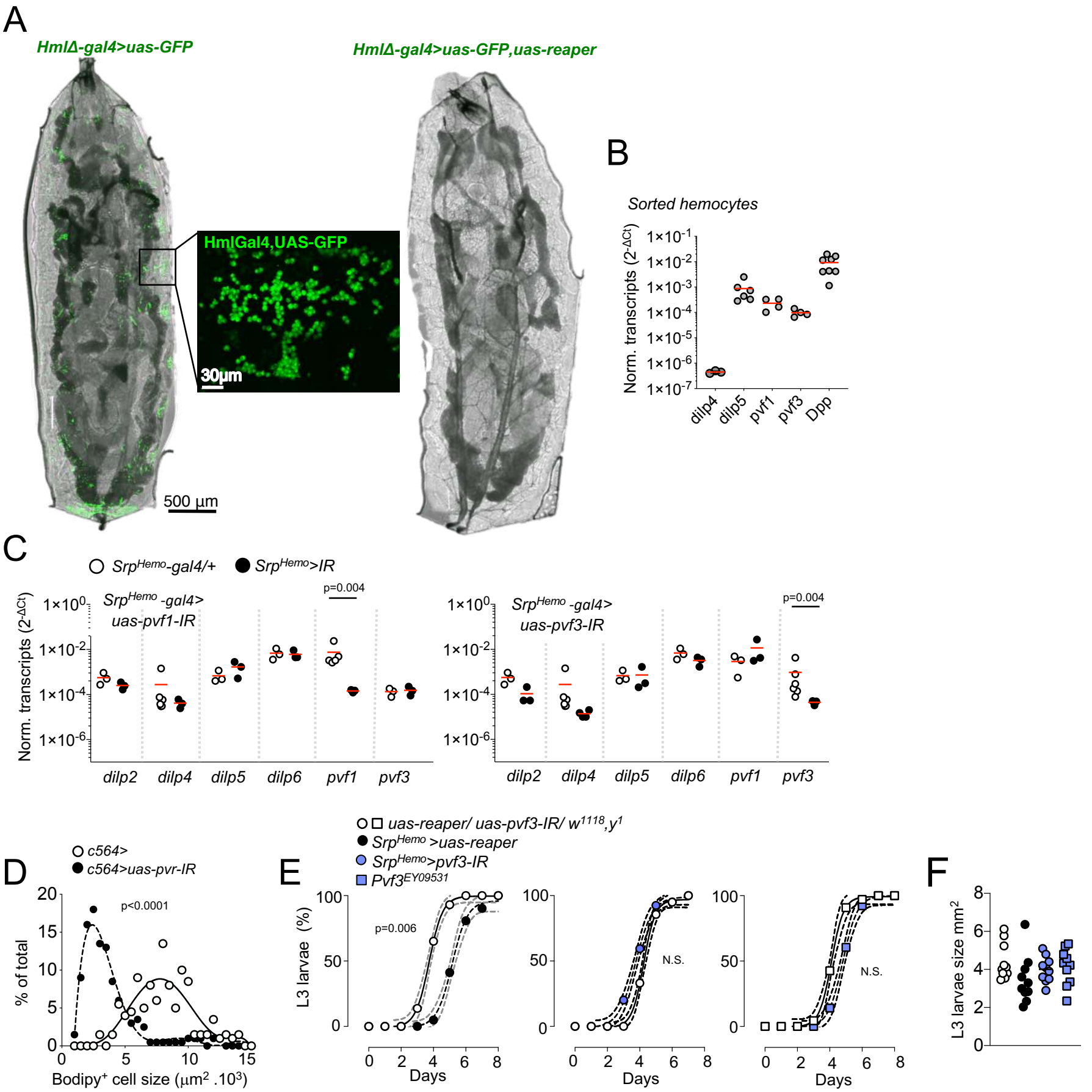

Analysis of hemocyte depletion and hemocyte specific *RNAi* of growth factors. (**A**) Confocal image of control (left, *Hml**Δ**-gal4>uas-GFP*) (n=10) and hemocyte-less L3 larvae (right, *Hml**Δ**-gal4>uas-GFP,uas-reaper*) (n=6). (**B**) qPCR analysis of the indicated growth factors in FACS-sorted hemocytes from *Hml**Δ**-gal4>uas-GFP* larvae. $2^{-\Delta Ct}$ is calculated relative to *Gapdh*, (n=4-9, 20 L3 larvae per replicate)**.** (**C**) qPCR analysis of the indicated growth factors in whole larvae in control *Srp^Hemo-gal4* L3 larvae, hemocyte specific RNAi of *pvf1* (left) and of *pvf3* (right), n=3-6 replicates, with 10 larvae per replicate**.** (**D**) Size distribution of Bodipy+ fat body cells in L3 larvae (n=3, from 3 crosses, 100-150 cells per replicate). p values obtained by t-test comparing mean cell size. (**E**) Developmental analysis of of the the larvae with the indicated genotype following egg deposition (n=3, from 30 larvae per replicate). The dashed lines indicate 95% confidence interval, p values obtained by t-test. (**F**) Size of L3 larvae from the indicated genotypes (n=10-20, from 5 larvae per replicate).

Fig. S7

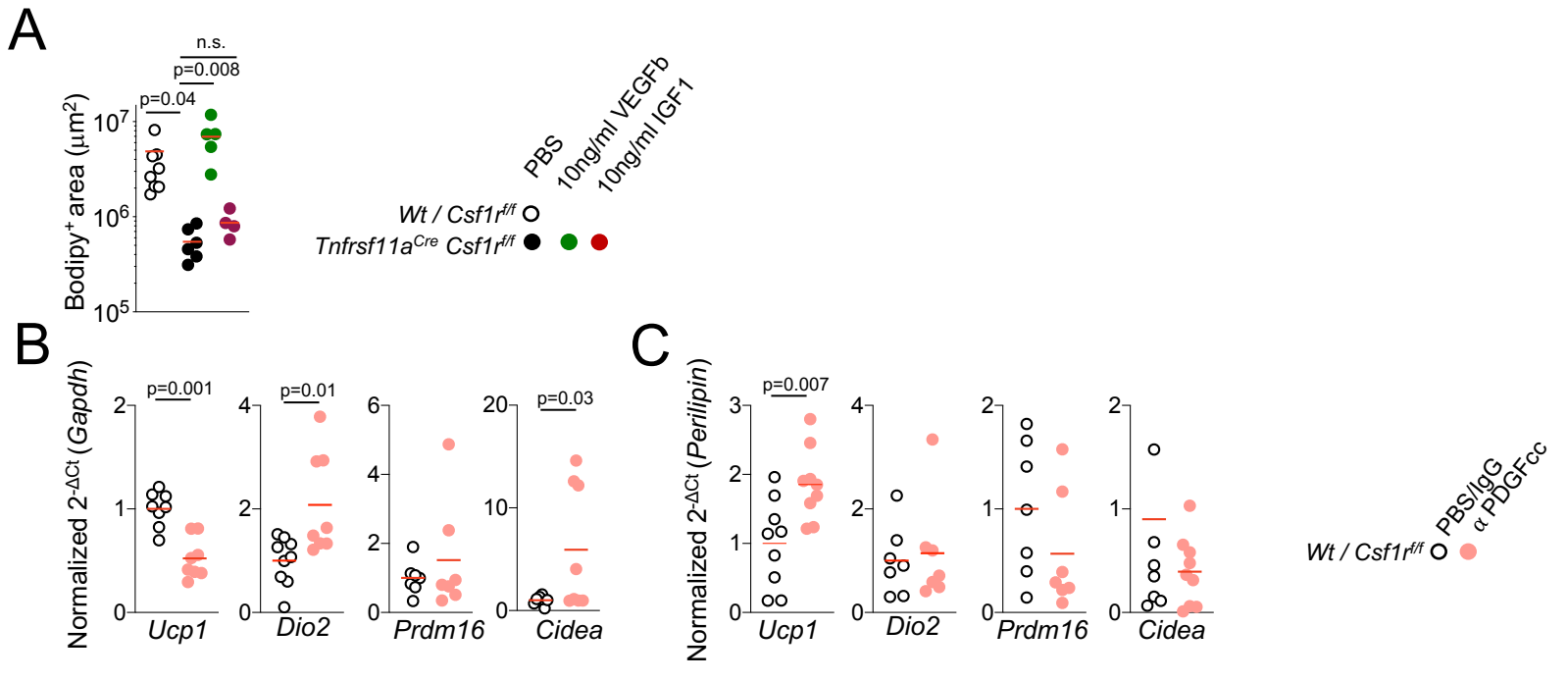

Analysis of eWAT explants. (**A**) Quantification of Bodipy$^+$ area from the indicated eWAT explants culterued for 10 days (n=4-7). p values obtained by one-way ANOVA with Sidak's correction. (**B**) qPCR analysis of the indicated genes in total eWAT explants (n=7-8). $2^{-\Delta Ct}$ calculated relative to *Gapdh* , p values obtained by t-test. (**C**) qPCR analysis of the indicated genes in total eWAT explants (n=7-9). $2^{-\Delta Ct}$ calculated relative to *Perilipin*, p values obtained by t-test.

Fig. S8

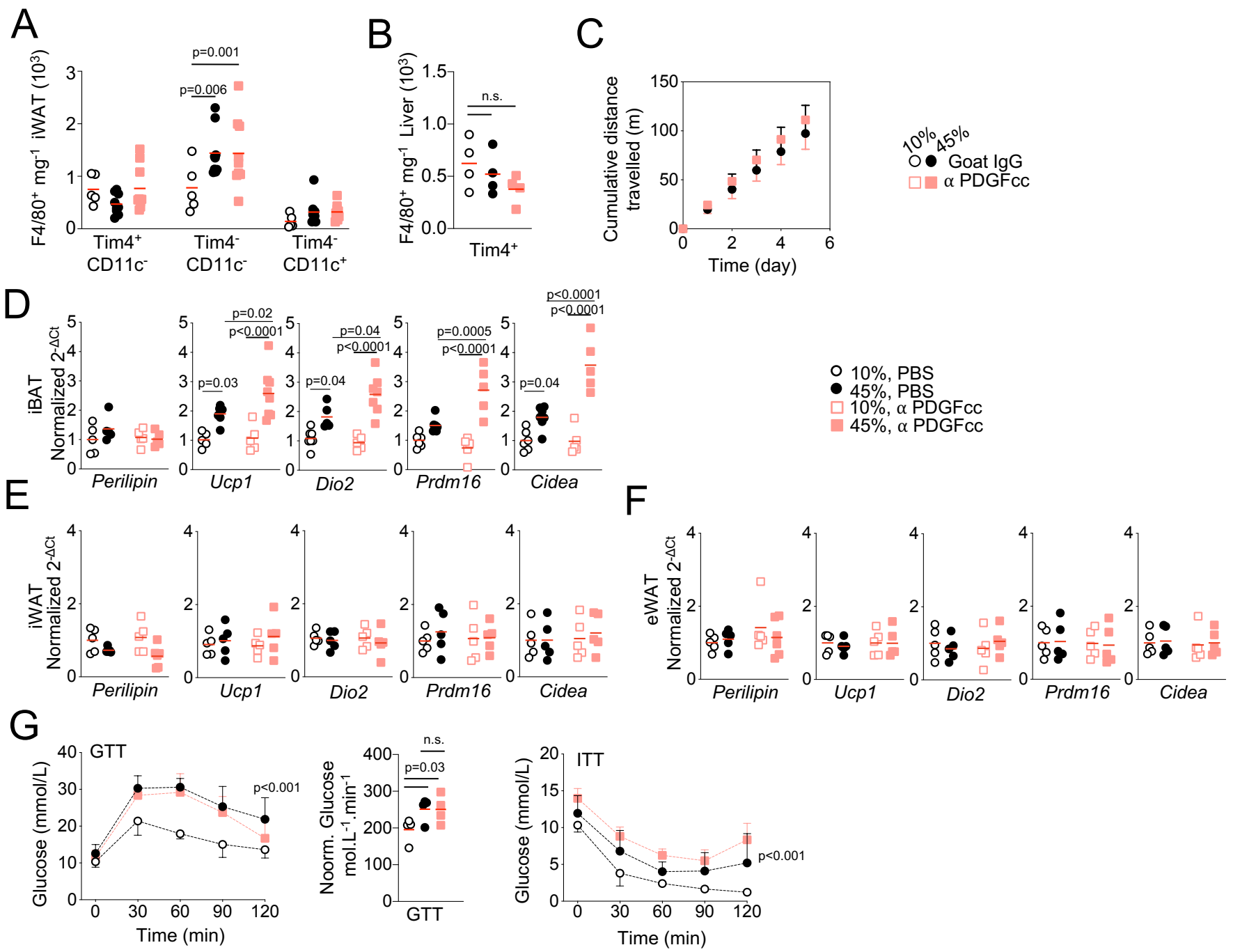

Characterization of C57Bl/6J mice injected with anti-PDGFcc neutralizing antibodies for 6-weeks. (**A**) Flow cytometry quantification of iWAT adipose tissue macrophages from C57Bl/6J mice fed the indicated diet and injected with anti-PDGFcc antibodies or goat IgG (n=5 for 10%, n=9 for 45%, and n=9 for 45% + anti-PDGFcc antibody). Each dot represents one mouse, p values obtained by one-way ANOVA with Sidak's correction. (**B**) Flow cytometry quantification of liver Kupffer cells from C57Bl/6J mice fed the indicated diet and injected with anti-PDGFcc antibodies or goat IgG (n=4). (**C**) Cumulative ambulatory activity was acquired using a laser matrix over a period of 5 days during the first week of anti-PDGFcc blocking antibodies or goat IgG treatment (n=8). Each dot represents the mean ± SD. (**D**) qPCR analysis of the indicated transcripts in iBAT of 12-week-old C57Bl/6J mice injected with anti-PDGFcc antibodies or goat IgG for 6 weeks (n=5-7). $2^{-\Delta Ct}$ calculated relative to *Gapdh,* p values obtained by one-way ANOVA with Sidak's correction. (**E,F**) qPCR analysis of the indicated transcripts in iWAT and eWAT of 12-week-old C57Bl/6J mice injected with anti-PDGFcc antibodies or goat IgG for 6 weeks (n=5-7). $2^{-\Delta Ct}$ calculated relative to *Gapdh*. (**i**) Representative H&E staining of livers from mice on the indicated diet and treatment (n=4 from 2 independent experiments). (**G**) Glucose Insulin and tolerance test on 12-week-old mice with the indicated diet and treatment (n=4). Each dot represents the mean ± SD. Each dot represents one mouse, p value obtained by t-test. Blood glucose concentration from the glucose tolerance test was normalized to the initial blood glucose level (time =0) and then the area under the curve was measured (n=4). Each dot represents one area under the curve from one mouse, p values obtained by one-way ANOVA with Sidak's correction.

Fig. S9

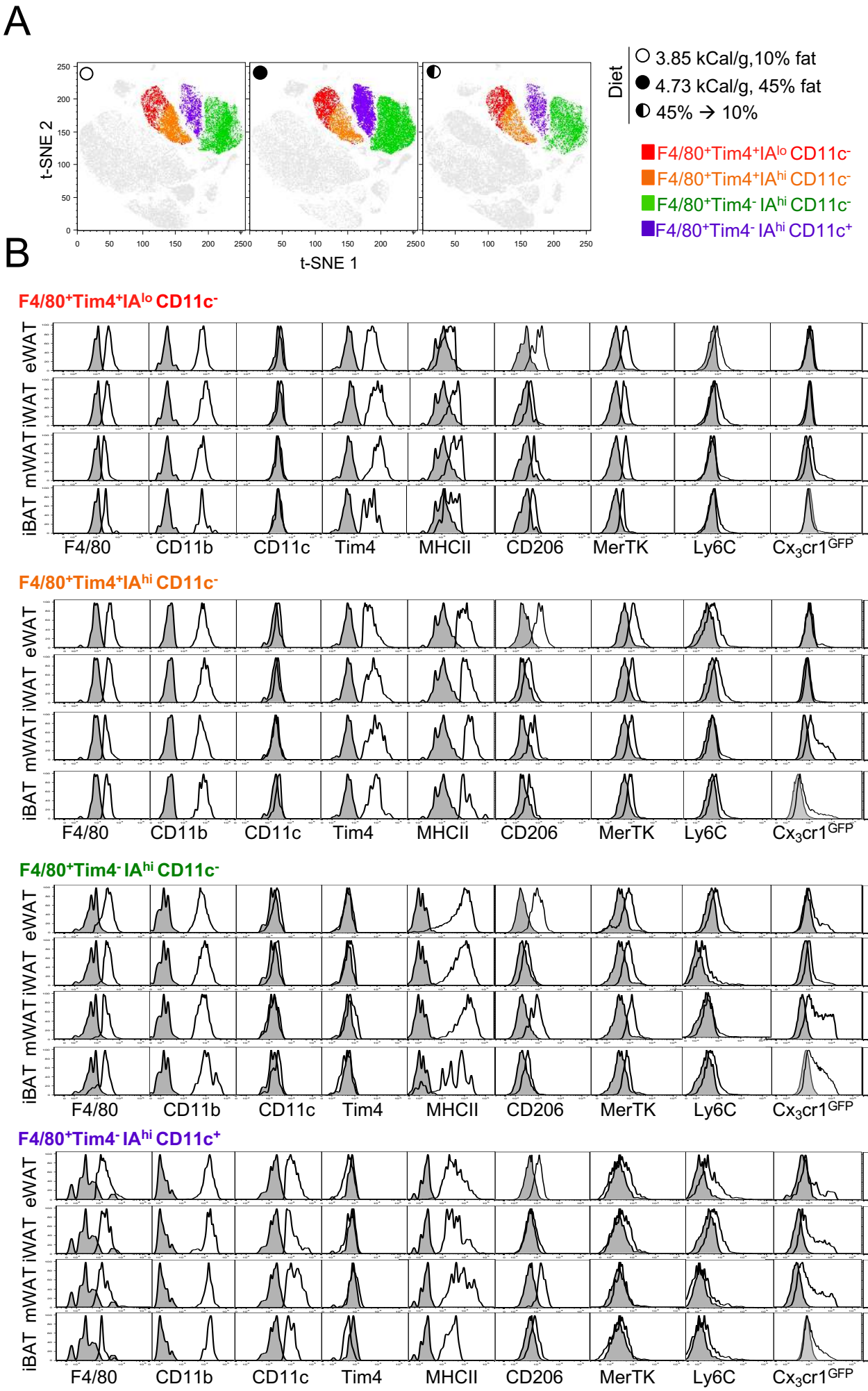

tSNE analysis of iWAT C57Bl/6J. (A) tSNE analysis of flow cytometry data for stromal vascular fraction from the iWAT of 14-week-old *C57Bl/6J* mice fed the indicated diet. The t-SNE algorithm was calculated on the singlets using the parameters: CD45, CD3, CD19, NKp46, SiglecF, Ly6G, F4/80, CD11b, Tim4, CD11c and MHCII, as well as FSC-A and SSC-A (representative of n=15). **(B)** Flow cytometry characterization of Tim4$^+$ and Tim4$^-$ macrophages color-coded in the tSNE plot in lean 8 weeks old mice. For F4/80, CD11b, CD11c, Tim4 and MHCII FMO were used. Anti-CD64, MerTK and Ly6C were compared to isotypes controls. The FMO and isotype controls were prepared from a mix of cells from the different adipose tissues and used to compare the expression of markers in all tissues. Expression of Cx3cr1 is measured in the $Cx_3cr1^{GFP/+}$ mice at 2 months of age and compared to a littermate controls (n=3).

Fig. S10

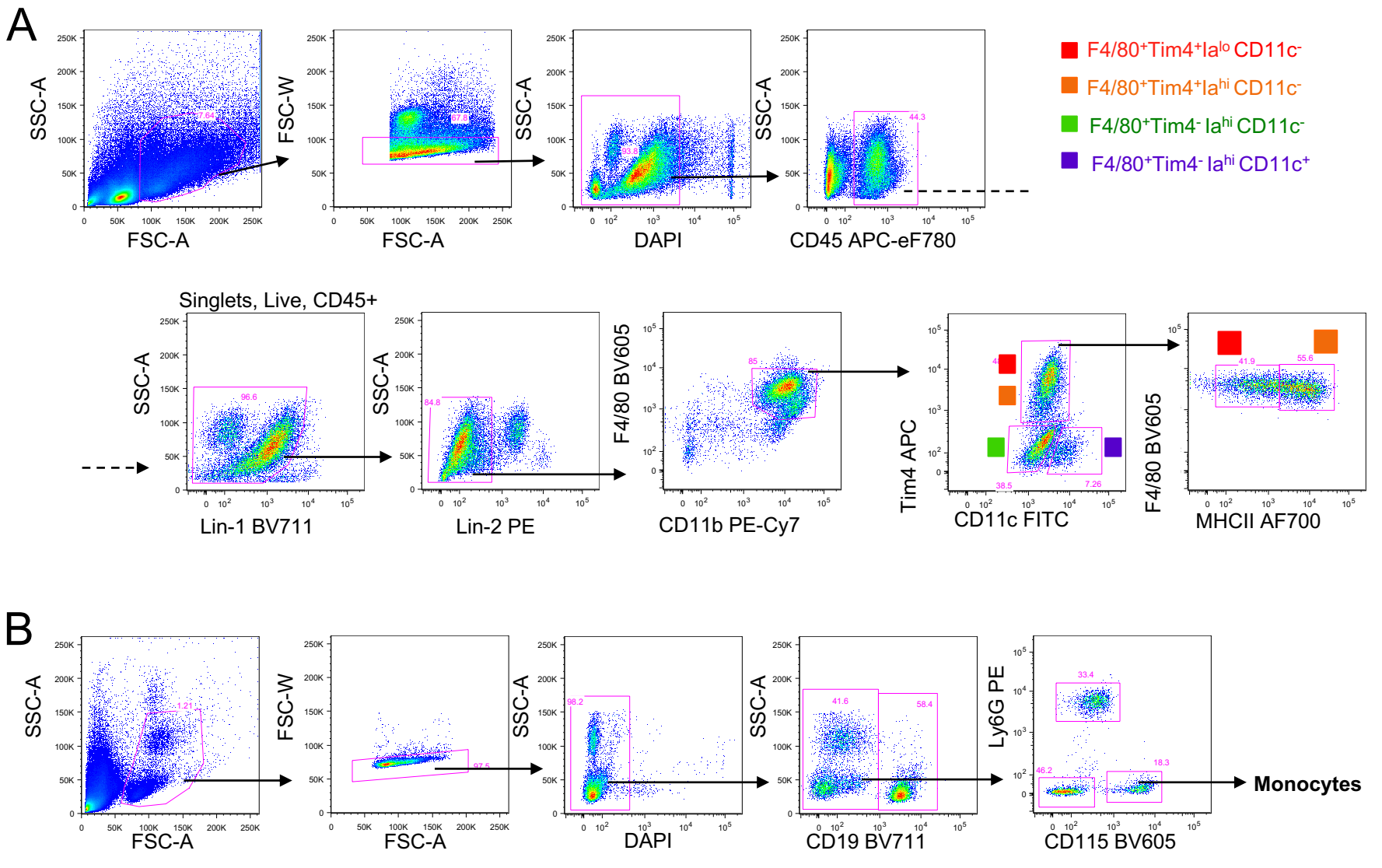

Gating strategy used for flow cytometry analysis of myeloid populations in the adipose tissue or blood. (**A**) Gating strategy used for flow analysis and flow sorting of different macrophage populations in the adipose tissues studied, the eWAT is represented here (representative of n=15). The same gating was used in iWAT, mWAT and iBAT as well. Lin-1 is CD3 CD19 NKp46, Lin-2 is SiglecF Ly6G. (**B**) Gating strategy for analysis of the blood Ly6C^{hi} monocytes.

Fig. S11

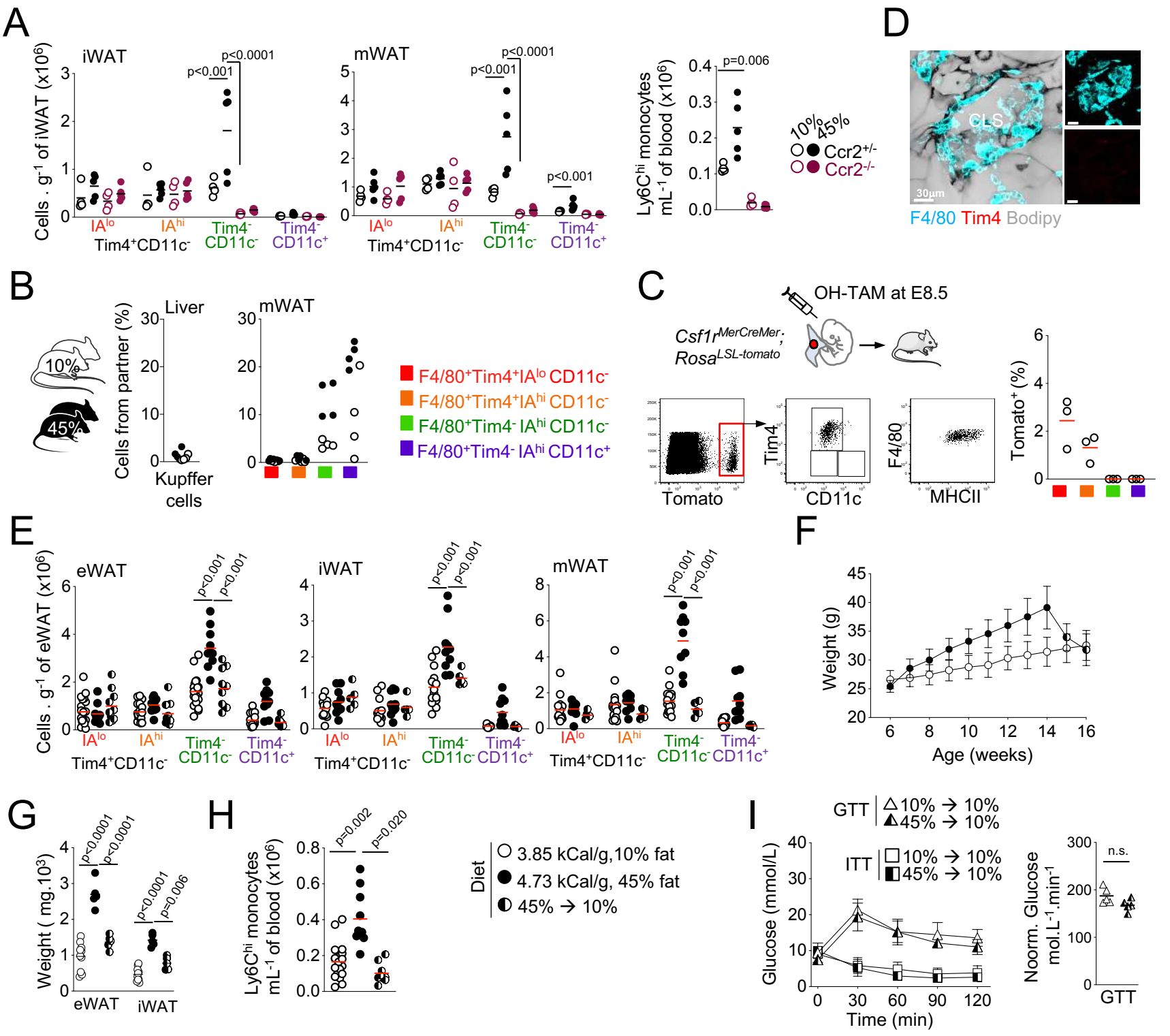

Characterization of different macrophage subsets in mice of 10% or 45% lipid diet. (**A**) Quantification of Tim4$^+$ and Tim4$^-$ macrophage populations in iWAT, and mWAT by flow cytometry in *Ccr2*$^{-/-}$ mice (n=4, from 2 litters) and littermate controls (n=5, from 2 litters) fed 10% or 45% lipid diet. Flow cytometry quantification of the blood Ly6C^{hi} monocytes (n=4-5 , from 2 litters). (**B**) Flow cytometry analysis of liver Kupffer cells and adipose tissue macrophages from mWAT of parabiotic pairs between CD45.1 and CD45.2 females fed 10% or 45% lipid diet. 2 pairs were analyzed per group. (**C**) Flow cytometry analysis of eWAT from 1-month-old *Csf1r*^{MeriCreMer};*Rosa*$^{LSL\text{-}tomato}$ mice pulse labelled with 4-hydroxy tamoxifen at E8.5. (Flow plot representative of n=4, from 2 litters). (**D**) Fluorescent whole mount image of adipose tissue macrophages in the iWAT of 14-week-old C57Bl/6J mice fed a 45% lipid diet for 8 weeks (representative of n=15), CLS denotes crown-like structures. (**E**) Quantification of Tim4$^+$ and Tim4$^-$ macrophage populations in eWAT, iWAT and mWAT by flow cytometry in C57Bl/6J mice fed 10% (n=10), 45% (n=9), or 45%>10% (n=9) lipid diet. (**F**) Mouse body weight, mean ± SD, n=10 for 10% and 45%, n=5 for 45%->10% of C57BL/6J mice fed the indicated diet. (**G**) Weight of adipose tissues from mice fed the indicated diet as in **E** and **F.** (**H**) Flow cytometry quantification of the blood Ly6C^{hi} monocytes (n=10 for 10%, n=9 for 45%, and n=9 for 45%>10%). (**I**) Insulin and glucose tolerance test in C57BL/6J mice (Each dot represents the mean ± SD, n=5) fed the indicated diet for 8 weeks and then switched to 10% fat diet. Blood glucose concentration from the glucose tolerance test was normalized to the initial blood glucose level (time =0) and then the area under the curve was measured (n=4), p values obtained by t-test. Each dot represents one mouse, p values obtained by one-way ANOVA unless otherwise stated.

Fig. S12

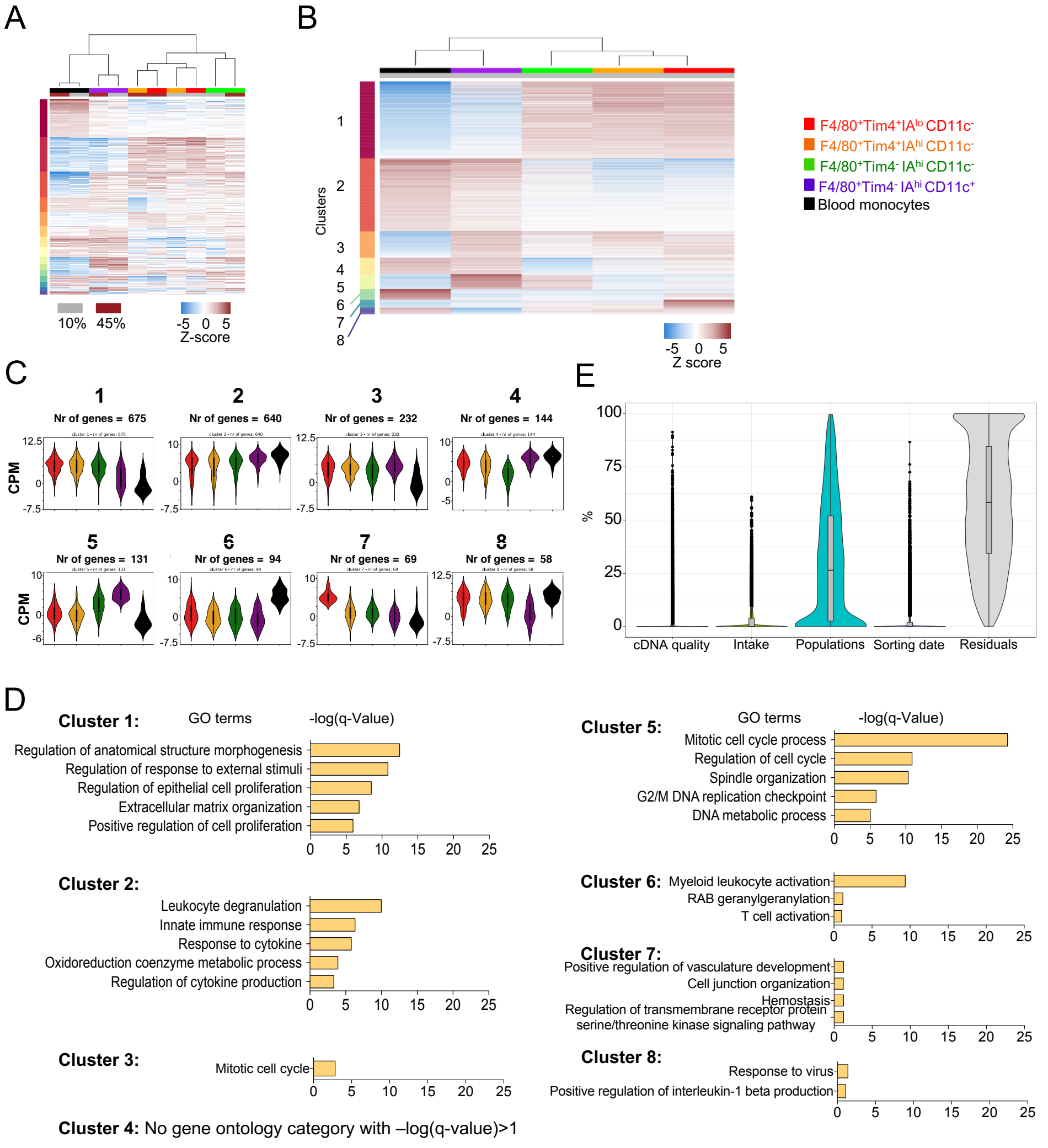

RNAseq analysis of C57Bl/6J male mice fed 10% or 45% lipid diet for 8 weeks. (**A**) Heatmap of differentially expressed genes in the color-coded macrophage subsets and blood monocytes from C57Bl/6J mice fed the indicated diet. Heatmap depicts z-scores. (**B,C**) Heatmap depicting clusters of differentially expressed genes. Heatmap depicts z-scores. Counts per million (CPM) for each sample in the different clusters. Number above depicts the cluster number. (**D**) Tables depicting significantly expressed gene ontology categories for cluster 3, 4, 6, 7 and 8. Only the gene ontology categories with a –log(q-value) superior to 1 are represented. (**E**) Violin plot representing the part of the variance explained by the difference between the populations, differences between the diets, different sorting dates, or quality of the samples.

Fig. S13

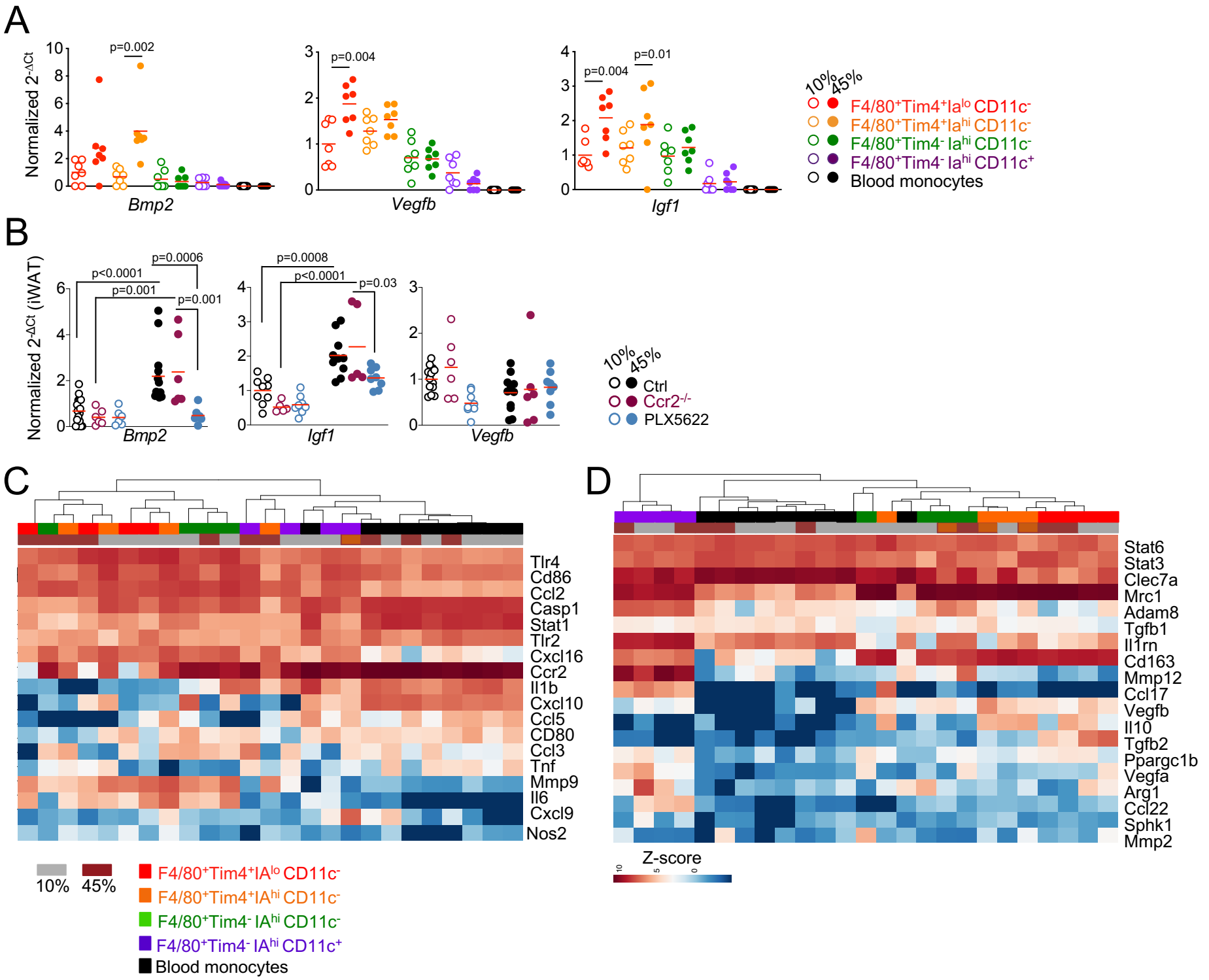

Characterization of different macrophage subsets in mice of 10% or 45% lipid diet. (**A**) Expression of indicated genes, relative to *Gapdh* and *Actinb* ($2^{-\Delta Ct}$), as determined by qPCR in FACS-sorted WAT macrophage subsets, and blood monocytes in C57Bl/6J fed a 10% or 45% lipid diet for 8 weeks (n=7 for adipose macrophages, n=9 for monocytes). (**B**) qPCR analysis of *Bmp, Igf1, and Vegfb* transcripts from the iWAT of C57BL/6J mice (n=9-17 for 10%, n=10-13 for 45%), *Ccr2*$^{-/-}$ (n=5-6 for 10%, n=5-6 for 45%), PLX5622-treated mice (n=6-8 10% + PLX5622, n=7-8 45% + PLX5622) and and controls fed 10% or 45% lipid diet for 8 weeks, normalized to *Gapdh.* Each dot represents one mouse, p values obtained by one-way ANOVA with Tukey's correction. (**C,D**) Heatmap representation of expression in the different populations in 10% or 45% lipid diets (n=2) for genes associated with (left)M1 or (right) M2 polarization of macrophages (Shaul et al, Diabetes 2010). Each column is color-coded. Heatmap depicts z-scores.

Fig. S14

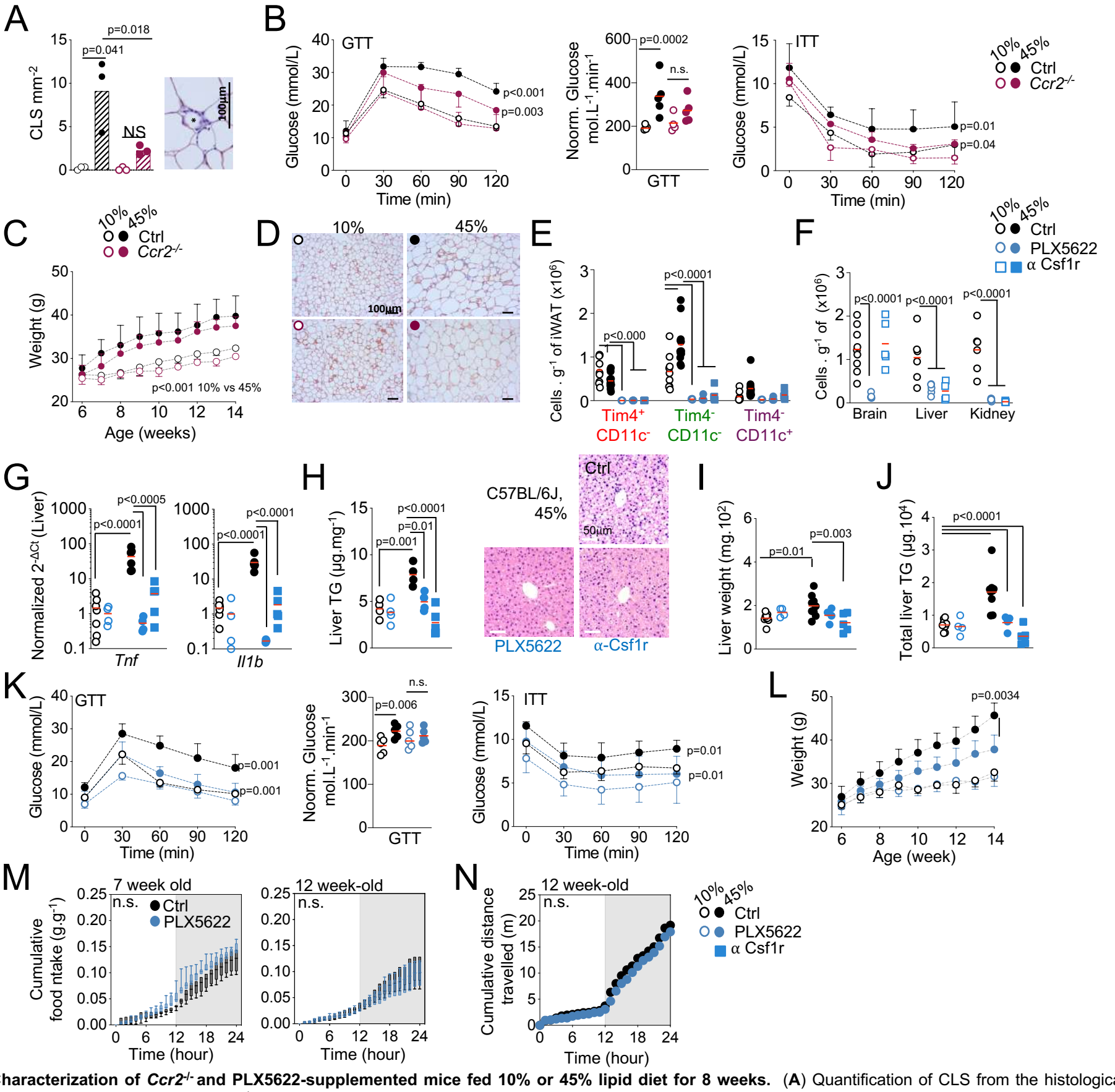

Characterization of *Ccr2*$^{-/-}$ and PLX5622-supplemented mice fed 10% or 45% lipid diet for 8 weeks. (**A**) Quantification of CLS from the histological section of iWAT taken from *Ccr2* $^{-/-}$ and littermate controls (n=3). Photograph of a Crown-like structure (CLS), denoted by asterisk, from perilipin stained paraffin embedded sections of iWAT from mice fed a 45% lipid diet. (**B**) Glucose and insulin tolerance test on *Ccr2* $^{-/-}$ and littermate control mice fed 10% (n=4) lipid diet or 45% (n=5) lipid diet for 8 weeks. Each dot represents the mean ± SD. p values obtained by t-test comparing the area under the curves for the indicated groups. Blood glucose concentration from the glucose tolerance test was normalized to the initial blood glucose level (time =0) and then the area under the curve was measured. Each dot represents one area under the curve from one mouse. (**C**) Mouse body weight (Each dot represents the mean ± SD, n=5) of *Ccr2* $^{-/-}$ mice and littermate controls fed 10% lipid diet or 45% lipid diet for 8 weeks. (**D**) Perilipin staining of paraffin embedded iWAT section from *Ccr2* $^{-/-}$ mice and littermate controls fed 10% lipid diet or 45% lipid diet for 8 weeks (n=4 for 10%, n=5 for 45% from 2 litters). (**E**) Flow cytometry quantification of iWAT adipose tissue macrophages from 14-week-old C57Bl/6J mice (n=9 for 10%, n=13 for 45% from 3 experiments) fed the indicated diet for 6-8 weeks and treated with PLX5622 (n=4 for 10% and 45%), a-CSF1R blocking antibodies (n=5 for 45%), or vehicle/IgG control. (**F**) Flow cytometry quantification of macrophages in the brain, liver, and kidney of C57Bl/6J mice fed PLX5622 (n=5), i.p injected with anti-CSF1R (AFS98) antibodies (n=4-5), or vehicle control for one week (n=6-10). (**G**) qPCR analysis of *Tnf* and *Il1b* transcripts in the liver of mice fed 10% or 45% fat diet with the indicated treatment(n=4-6), normalized to *Gapdh* (2-ΔCt). (**H**) Liver Triglycerides per mg of tissue in mice on the indicated diet (n=4-5). Representative H&E staining of livers from C57BL/6J mice on the indicated diets. (**I**) Liver weight of C57Bl/6J mice fed the indicated diet with the denoted treatment for 8 weeks(n=4-7). (**J**) Total Liver Triglycerides in mice on the indicated diet (n=4-9). (**K**) Glucose and insulin tolerance test on mice fed 10% lipid diet or 45% lipid diet with/without PLX5622 for 8 weeks (n=5). Each dot represents the mean ± SD. p values obtained by t-test comparing the area under the curves for the indicated groups. Blood glucose concentration from the glucose tolerance test was normalized to the initial blood glucose level (time =0) and then the area under the curve was measured (n=5). Each dot represents one area under the curve from one mouse. (**L**) Mouse body weight over time fed the indicated diet (10% lipid diet group n=5, 45% lipid diet group n=7, 10% lipid diet group + PLX5622 n=5, 45% lipid diet group + PLX5622 n=10). Mean ± SD, p values at 14 weeks of age obtained by t-test. (**M**) Cumulative food intake was measured gravimetrically in 7 and 12-week-old C57Bl/6J mice fed the indicated diet (n=8). (**N**) Cumulative ambulatory activity was acquired using a laser matrix, each dot represents mean ± SD of n=8.
Each dot represents one mouse, p values obtained by one-way ANOVA unless otherwise stated.

Fig. S15

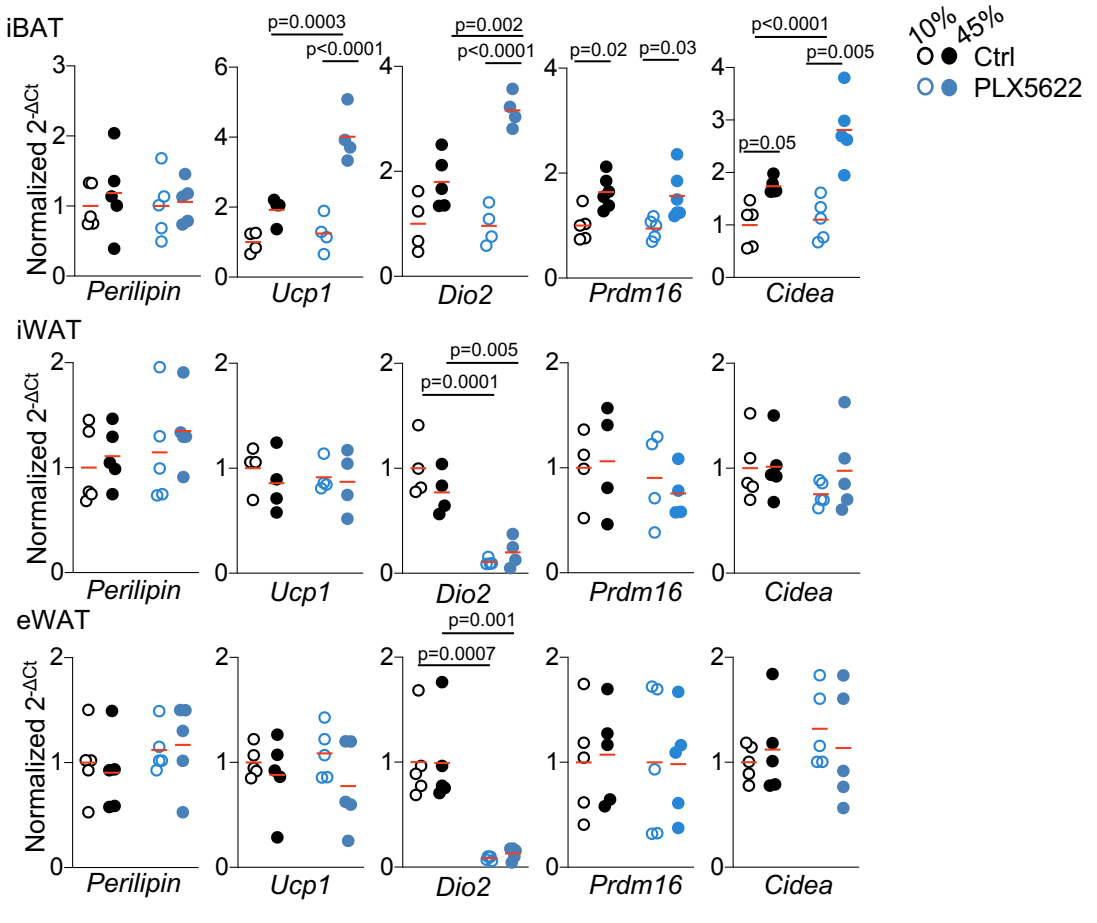

qPCR analysis of iBAT, iWAT, and eWAT in PLX5622 treated mice. qPCR analysis of the indicated genes from the iBAT, iWAT, and eWAT of mice fed 10% or 45% lipid diet for 8 weeks (n=4-5), normalized to *Gapdh.* Each dot represents one mouse, p values are obtained by one-way ANOVA with Sidak's correction.

Fig. S16

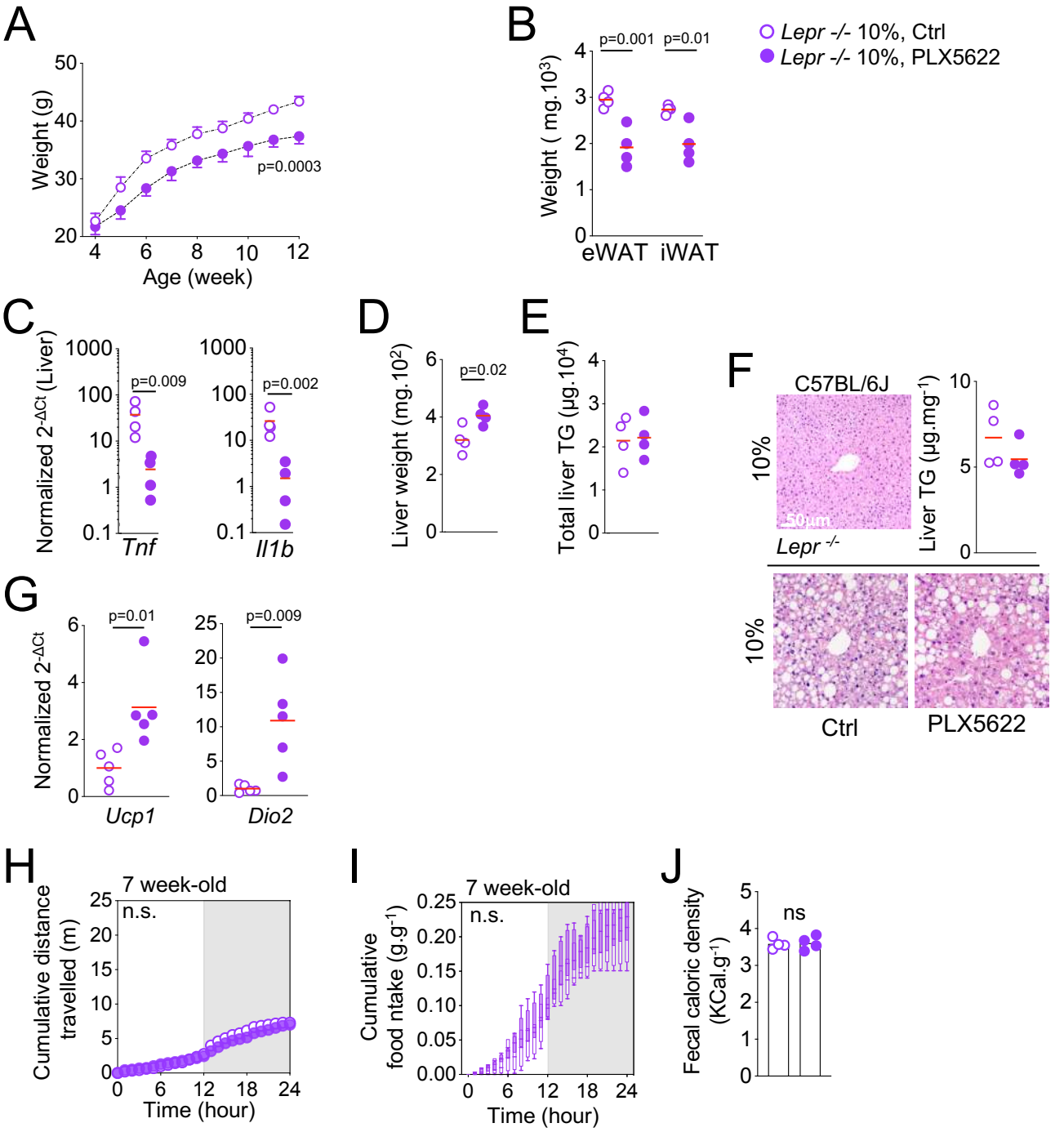

Characterization of *Lepr*$^{-/-}$ mice supplemented with PLX5622 fed 10% or 45% lipid diet for 8 weeks. (**A**) Mouse body weight (Each dot represents the mean ± SD, n=4) of *Lepr*$^{-/-}$ mice fed 10% lipid diet + PLX5622 or 10% lipid diet for 8 weeks. p values at 12 weeks of age obtained by t-test. (**B**) Weight of adipose tissues from 12-week-old *Lepr* $^{-/-}$ mice fed the indicated diet for 8 weeks (n=4). p values obtained by one-way ANOVA with Sidak's correction. (**C**) qPCR analysis of *Tnf* and *Il1b* transcripts in the liver of mice fed 10% fat diet with the indicated treatment (n=4), normalized to *Gapdh* ($2^{-\Delta Ct}$). (**D**) Liver weight of *Lepr*$^{-/-}$ mice fed the indicated diet for 8 weeks (n=4). (**E**) Total Liver Triglycerides in mice on the indicated diet (n=4). (**F**) Representative H&E staining of livers from mice on the indicated diets. Liver Triglycerides per mg of tissue in mice on the indicated diet (n=4). (**G**) qPCR analysis of *Ucp1* and *Dio2* in the iBAT mice treated with/without PLX5622 (n=4). Data is normalized to *Gapdh* for calculation of the $2^{-\Delta C}$. (**H**) Cumulative ambulatory activity was acquired using a laser matrix, each dot represents mean ± SD of n=4. (**I**) Cumulative food intake was measured gravimetrically in 7-week-old *Lepr* $^{-/-}$ mice fed the indicated diet (n=4). (**J**) Feces were collected from 7-week-old *Lepr* $^{-/-}$ mice fed the indicated diet and then subjected to bomb calorimetry to measure fecal caloric density (n=4).
Each dot represents one mouse. p values obtained by t-test unless otherwise stated.